

# ALFALFA and WSRT Imaging of Extended H I Features in the Leo Cloud of Galaxies

Lukas Leisman,<sup>1</sup> Martha P. Haynes,<sup>1</sup> Riccardo Giovanelli,<sup>1</sup> Gyula Józsa,<sup>2,3,4</sup>  
Elizabeth A. K. Adams,<sup>5</sup> Kelley M. Hess<sup>5,6</sup>

<sup>1</sup>*Cornell Center for Astrophysics and Planetary Science, Space Sciences Building, Cornell University, Ithaca, NY 14853, USA*

<sup>2</sup>*SKA South Africa Radio Astronomy Research Group, 3rd Floor, The Park, Park Road, Pinelands 7405, South Africa*

<sup>3</sup>*Rhodes Centre for Radio Astronomy Techniques & Technologies, Department of Physics and Electronics, Rhodes University, PO Box 94, Grahamstown 6140, South Africa*

<sup>4</sup>*ArgelanderInstitut für Astronomie, Auf dem Hügel 71, D-53121 Bonn, Germany*

<sup>5</sup>*ASTRON, the Netherlands Institute for Radio Astronomy, Postbus 2, 7990 AA, Dwingeloo, The Netherlands*

<sup>6</sup>*Kapteyn Astronomical Institute, University of Groningen, PO Box 800, NL-9700 AV Groningen, The Netherlands*

Accepted 2016 August 17. Received 2016 August 12; in original form 2016 May 18

## ABSTRACT

We present ALFALFA H I observations of a well studied region of the Leo Cloud, which includes the NGC 3227 group and the NGC 3190 group. We detect optically dark H I tails and plumes with extents potentially exceeding 600 kpc, well beyond the field of view of previous observations. These H I features contain  $\sim 40\%$  of the total H I mass in the NGC 3227 group and  $\sim 10\%$  in the NGC 3190 group. We also present WSRT maps which show the complex morphology of the extended emission in the NGC 3227 group. We comment on previously proposed models of the interactions in these groups, and the implications for the scale of group processing through interactions. Motivated by the extent of the H I plumes, we place the H I observations in the context of the larger loose group, demonstrating the need for future sensitive, wide field H I surveys to understand the role of group processing in galaxy evolution.

**Key words:** galaxies: evolution - - galaxies: groups: individual: (NGC 3190, NGC 3227, HCG 44) - - radio lines: galaxies

## 1 INTRODUCTION

Most galaxies at  $z \sim 0$  can be found in group environments (e.g. Tago et al. 2008), where evidence of tidal interactions and gas stripping are particularly prevalent (e.g. Hibbard et al. 2001a; Hibbard et al. 2001b). These observations of ongoing tidal interactions suggest that galaxies can undergo significant morphological evolution in the group environment, possibly playing a major role in the morphology-density relation (e.g. Postman & Geller 1984; Bekki & Couch 2011; Hess & Wilcots 2013).

H I observations can give direct evidence to the fundamental role of group processing in galaxy evolution, tracing the recent interaction history of group galaxies (e.g. Yun et al. 1994). However, while the inner interactions of merging galaxies have been observed in detail, (e.g. Rand 1994), H I studies covering the full extent of interactions in groups are difficult to execute due to the need for high sensitivity over wide fields; wide field H I surveys have been limited in resolution and sensitivity, and interferometric studies have been limited to the field of their primary beam.

Still, H I mapping on the group scale is important for

understanding the ubiquity of these interactions, the fraction of gas involved, and the interaction time scales (e.g., Serra et al. 2015), which in turn constrain the impact of tidal processing in groups on galactic evolution, relative to other processes, like the decrease in cold gas accretion (Sancisi et al. 2008).

The Arecibo Legacy Fast ALFA (Arecibo L-band Feed Array) survey (ALFALFA; Giovanelli et al. 2005) provides high sensitivity, unbiased, wide field maps of H I in the local volume, and has traced the atomic gas distribution in a variety of local groups (Stierwalt et al. 2009; Lee-Waddell et al. 2012; Lee-Waddell et al. 2014).

Here we present the ALFALFA data on a well studied loose group in the Leo Cloud, known to show significant evidence of interaction. The ALFALFA data are not limited to an arbitrary region on the sky, allowing us to search for additional structures and constrain the cold gas fraction outside stellar disks over the full  $\sim 9$  Mpc<sup>2</sup> physical region. These data reveal substantial intragroup cold gas, demonstrating the power of sensitive, wide field H I mapping.

We summarize prior work on this group in section 2 and present our observations in section 3. We present our

results in section 4, discuss the group context in section 5 and conclude in section 6. For all calculations, the assumed cosmology is  $H_0 = 70 \text{ km s}^{-1} \text{ Mpc}^{-1}$ ,  $\Omega_m = 0.3$ , and  $\Omega_\Lambda = 0.7$ .

## 2 PLACEMENT IN THE COSMIC WEB

### 2.1 The NBG 21-6 Region

Figure 1<sup>1</sup> shows the distribution of galaxies in the constellation Leo, between heliocentric recessional velocities of  $v_h = 700 \text{ km s}^{-1}$  and  $1700 \text{ km s}^{-1}$ . The primary structure in this velocity range is the Leo Cloud,<sup>2</sup> a loose collection of groups stretching  $\sim 50^\circ$  across the plane of the sky at a distance of  $\sim 20\text{--}30 \text{ Mpc}$ , from the edge of the Virgo Cluster around  $12^h + 15^\circ$  (the lower left corner of Figure 1), to around  $9^h 30^m + 35^\circ$  (the upper right corner). A region of particular interest for H I studies (see section 2.3) is a loose association of galaxies spanning  $\sim 6 \text{ Mpc}$  in the NW part of the Leo Cloud (indicated with a dashed circle in Figure 1). Figure 2 shows the velocity distribution of H I sources in this region, which is approximately Gaussian, with an average heliocentric recessional velocity of  $1304 \text{ km s}^{-1}$ , and a dispersion of  $\sigma \sim 115 \text{ km s}^{-1}$ , in contrast with the more uniform distribution of the Leo Cloud at large.

Yet, the group relationships of galaxies in this region is unclear. Several studies assign the galaxies in this region to a single group (e.g., Huchra & Geller 1982; Garcia 1993), which we will refer to as NBG 21-6 following the nomenclature of the Nearby Galaxies Catalog (Tully 1987). However, depending on the length scale chosen to link the galaxies, other authors have divided this region into two subgroups (e.g., Turner & Gott 1976; Geller & Huchra 1983), as indicated by the dash-dotted line in Figure 1, and still others further divide the SW subgroup (pictured in Figure 3) into the NGC 3227 group, and the NGC 3190 group (e.g., Makarov & Karachentsev 2011).

Figure 2 also shows the velocity distributions of the component NGC 3190 and NGC 3227 groups, which have mean recessional velocities (dispersions) of  $1220$  ( $99$ ) and  $1353$  ( $150$ )  $\text{km s}^{-1}$  respectively, in contrast with the distribution for the full NBG 21-6 region. Groups were assigned by selecting all sources within the boxed regions in Figure 3 (described in Section 4) within the stated velocity range. Tables 1 and 2 list the basic properties of the galaxies assigned to each group by this simplistic method (sources assigned to different groups by a more sophisticated algorithm (Makarov & Karachentsev 2011) are noted with a star). Both the shape and narrowness of the velocity distribution suggest a relationship between the sources in the

NBG 21-6, even while the precise nature of that relationship is uncertain.

### 2.2 Distances in the NBG 21-6 Region

Distance determinations to member galaxies compound the problem of group membership. Standard Hubble flow would give distances between 15 and 22 Mpc, but the entire region is falling into Virgo at  $\sim 200 \text{ km s}^{-1}$  (Karachentsev et al. 2015a), and individual galaxies are falling into the local filament and groups (see section 5.3). More, redshift-independent distance measurements for this group are both complicated and confusing. There are three sources with measured primary distances: NGC 3226 (23.6 Mpc) and NGC 3193 (34 Mpc) via surface brightness fluctuations (Tonry et al. 2001) and NGC 3190, which contains two type Ia supernovae that give distance estimates ranging from 18 (Amanullah et al. 2010) to 31 Mpc (Szabó et al. 2003) depending on calibration. However, given the strong interactions in this region, the primary distances to each of these objects may be strongly effected by systematic errors (see Serra et al. 2013 for a brief discussion). Other redshift-independent distances are little help, as estimates based on scaling relations are complicated by interactions; for example, estimates of distances to the merging pair NGC 3226/NGC 3227 range from 14.5 Mpc (Yoshii et al. 2014) to 43.5 Mpc (Blakeslee et al. 2001).

Thus, observations that bridge the gap between individual galaxies and the group structure are important for disentangling the complex relationships in this region. In section 5 we argue that the sources in this region are gravitationally interacting, and likely to be at a similar distance. Using the corrections given in the NASA Extragalactic Database, based on the local velocity field model from Mould et al. (2000), we estimate a distance of 24.3 Mpc from the average velocity of the NBG 21-6 group. We thus choose to follow Serra et al. (2013) and assume a distance of 25 Mpc for all galaxies in the region for the remainder of this paper. We further defend this choice in section 5.3.

### 2.3 Interactions in the NBG 21-6 Region

Previous studies have found significant evidence of interactions between group members in the NBG 21-6 region. The NGC 3190 group centers around Hickson Compact Group 44 (HCG 44), a compact group of four galaxies of similar optical brightness. Several studies have found that the galaxies in HCG 44 appear to be H I deficient (see section 5.1), and NGC 3187 and NGC 3190 show strong morphological evidence of tidal interactions. Moreover, Serra et al. (2013) report the discovery of a large  $\sim 300 \text{ kpc}$  H I tail extending to the north and west of the group.

Similarly, Mundell et al. (1995) found two tails stretching  $7'$  north and  $16'$  south (51 and 116 kpc at  $D=25 \text{ Mpc}$ ) of the interacting pair NGC 3226 and NGC 3227 (also called Arp 94) in deep C and D array VLA imaging. Optical imaging shows a complex set of faint stellar filaments, arcs, and loops, and Appleton et al. (2014) suggest a complex interaction history based on a plethora of multi-wavelength data.

While previous observations have been sufficient to reveal the complex nature of both the NGC 3227 and

<sup>1</sup> Data are taken from the Arecibo General Catalog (AGC), a private database maintained over the years by MPH and RG; it contains all bright galaxies and ones of known redshift as available in NED with  $cz < 18000 \text{ km s}^{-1}$  in the ALFALFA volume, additional unpublished H I results as they are acquired, and bright galaxies in other regions of the sky.

<sup>2</sup> Analysis of the Leo Cloud is complicated by the superposition of the foreground Leo Spur at  $\sim 10 \text{ Mpc}$ , which is poorly discriminated in velocity space due to infall toward the Virgo Cluster (e.g., Tully 1987; Karachentsev et al. 2015b). ALFALFA results for the southern part of the Leo Cloud were presented in Stierwalt et al. (2009), but the coverage there only extended to  $\delta < 16^\circ$ .

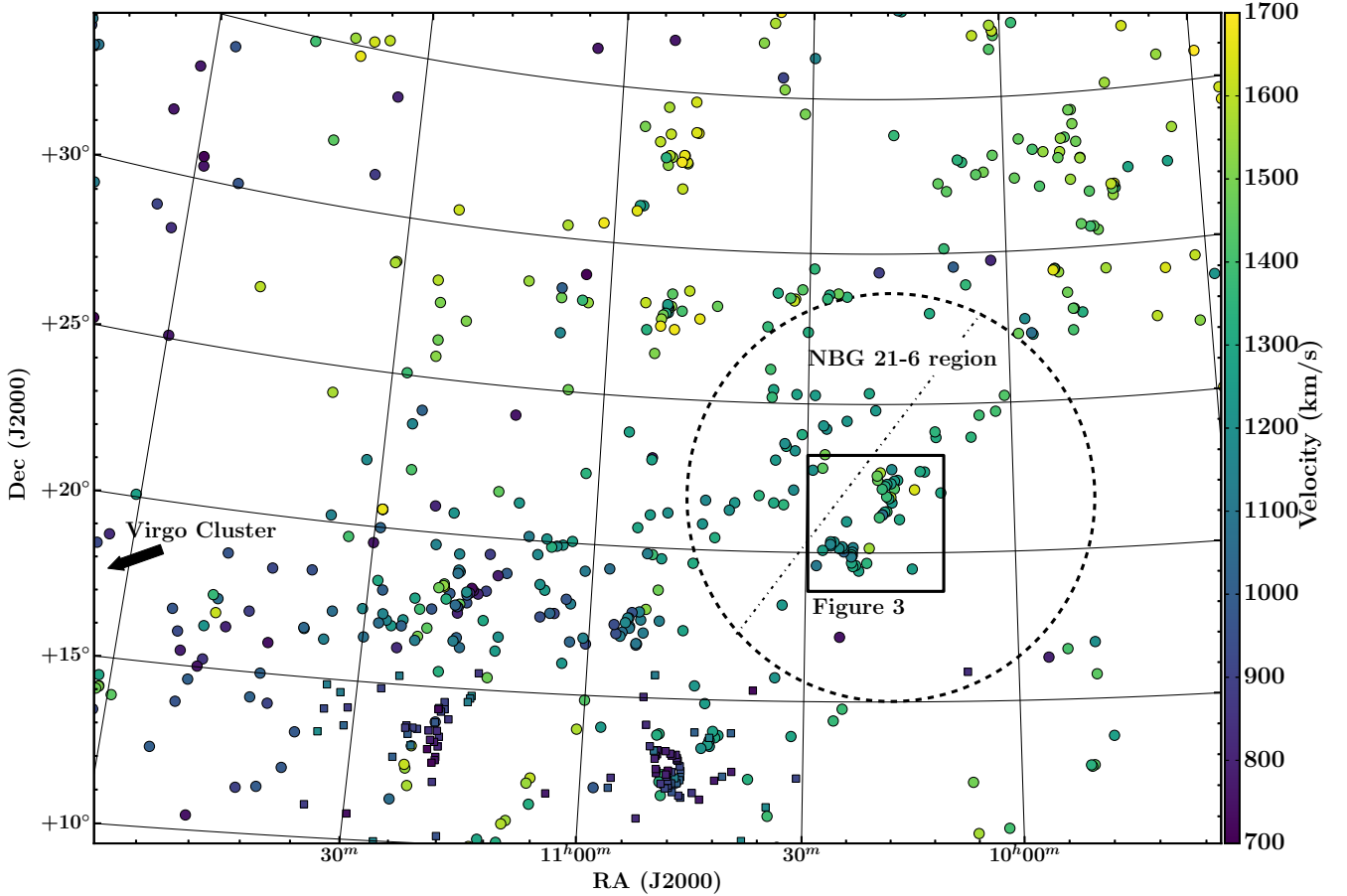


**Figure 1.** The distribution of galaxies in the NBG 21-6 region within the context of the Leo Cloud, a sparsely populated filament at  $D \sim 20$ – $30$  Mpc stretching from the lower left of the image (near the Virgo Cluster) to the upper right. Sources are colour coded by heliocentric recessional velocity, and show some gradient from high to low velocities as the filament approaches the Virgo Cluster. The dashed circle has a radius of 3 Mpc at a distance of 25 Mpc, and shows the location of the NBG 21-6 region that is the primary focus of this study. Some group catalogues divide the sources in the NBG 21-6 region into two subgroups, as indicated by the dashed-dotted line. The central/SW region (below the dashed-dotted line) itself has two main concentrations, the NGC 3227 and NGC 3190 groups (Figure 3), which contain the large H I structures discussed in section 4. Members of the foreground Leo Spur ( $D \sim 10$  Mpc), as identified by Stierwalt et al. (2009), are indicated by squares rather than circles.

NGC 3190 groups, they have been limited by the field of view of their observations. Here we present the the first high sensitivity, complete H I maps of then entire region, corroborating and extending these results (see sections 4.1 and 4.2 for the NGC 3227 and NGC 3190 subgroups respectively), and painting a global picture of H I in the region.

### 3 OBSERVATIONS AND DATA

#### 3.1 H I Data from the ALFALFA Survey

The ALFALFA observations and data processing are described in detail in previous papers (Giovanelli et al. 2005; Saintonge 2007; Martin et al. 2009; Haynes et al. 2011). In brief, ALFALFA employs a two-pass, fixed azimuth drift scan strategy, with a bandwidth of 100 MHz and a spectral resolution of 24.4 kHz ( $5.3 \text{ km s}^{-1}$  at  $z=0$ ) before Hanning smoothing. The data are bandpass subtracted, calibrated, and then flagged interactively for radio frequency interference (RFI). Once this “level 1” processing is complete, the

data are gridded into cubes  $2.4^\circ$  on a side and spanning the full spectral bandwidth from  $-2000$  to  $18,000 \text{ km s}^{-1}$  (though the cubes are split into four subcubes of 1024 spectral channels each for easy processing). Each cube was flat-fielded and rebaselined, and corrected for residual telescope pointing errors. Sources are extracted using the methods of Saintonge (2007), and then each grid is examined by eye to improve on the automatic detection algorithm at lower signal to noise ratios (SNRs) and to identify optical counterparts in Sloan Digital Sky Survey (SDSS) and Digitized Sky Survey 2 (DSS2) images; final source parameters are measured and catalogued interactively. The public 70% ALFALFA catalogue has  $>25,000$  high SNR extragalactic detections (Jones et al. 2016).

Due to their large angular extent, the structures discussed in this paper were originally split across multiple cubes. Thus, to better study the region on physically relevant scales, the ALFALFA data were regridded into a single  $50$  square degree cube centered at  $10^h20^m + 21^\circ$ . The moment 0 map of the central portion of this region is shown in Figure 3. This map was created by first smoothing to  $2\times$  the beam

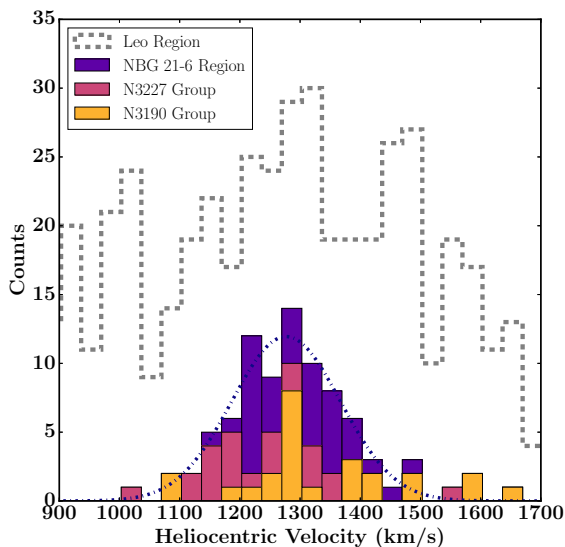


**Figure 2.** Histogram of heliocentric recessional velocities in the Leo Region. The filled purple bars indicate the counts for the NBG 21-6 region (dashed circle in Figure 1), which shows a roughly Gaussian distribution (the best fitting Gaussian with  $\sigma \sim 115 \text{ km s}^{-1}$  is overplotted as a dash-dotted line), in contrast with the source distribution for all sources in Figure 1, indicated here by the dashed grey line. Sources in the NGC 3190 (yellow) and NGC 3227 (pink) groups are subsets of the NBG 21-6 distribution.

size and then masking pixels below  $2.5\sigma$ . Actual telescope scheduling, gain differences between the ALFA beams, and significant flagging due to RFI resulted in uneven integration times and rms values across the cube. To correct for this we used a weights map of effective integration time after flagging to create an rms cube which allowed us to determine the appropriate threshold for masking. One strip in particular,  $\delta \sim 21^{\circ}38'$ , was strongly affected by low level RFI and required additional masking. The mask was then applied to the unsmoothed cube, which was then summed over velocity channels from 911 to  $1722 \text{ km s}^{-1}$ , encompassing the full velocity range of the sources in the group.

Total H I fluxes for all sources in the region were extracted manually using the standard ALFALFA software (see Haynes et al. 2011). However, the ALFALFA algorithm is optimized for point sources rather than highly extended and asymmetric sources like the features discussed below. Thus, all sources were remeasured by a modified version of the software which spatially integrates the spectrum over any arbitrary shaped area, and then divides by the summed value of the normalized beam over the same set of image pixels (e.g., Shostak & Allen 1980). This method gives consistent measurements with the standard software on point sources, and recovers up to  $\sim 20\%$  more flux for the extended sources in this field.

### 3.2 H I Synthesis Imaging with WSRT

Three sources in the vicinity of NGC 3226/7 were included in an exploratory sample of synthesis observations studying extreme H I sources without optical counterparts in ALFALFA (see Cannon et al. 2015 and Janowiecki et al. 2015 for more

details). The connection to NGC 3226/7 was noted, but the nature of the dark H I knots, given their large separations from the merging pair, was unclear.

We observed these three sources with  $4 \times 12 \text{ h}$  pointings with WSRT, 2 centered at  $10^{\text{h}}25^{\text{m}}21.0^{\text{s}} + 20^{\circ}10'05''$ , one centered at  $10^{\text{h}}22^{\text{m}}26.2^{\text{s}} + 19^{\circ}23'17''$  and one at  $10^{\text{h}}25^{\text{m}}55.0^{\text{s}} + 20^{\circ}20'33''$ . The primary beams of the three pointing centers are  $35'$  wide. We centered observations on the H I line in one band of 10 MHz bandwidth and 1024 channels in two polarizations. This resulted in a broad range of line free channels for continuum subtraction and a velocity resolution of  $4.1 \text{ km s}^{-1}$  (FWHM) after Hanning smoothing.

We reduced the data using the same automated pipeline as applied in Wang et al. (2013), originally used by Serra et al. (2012), as described in Janowiecki et al. (2015). The pipeline uses the data reduction software Miriad (Sault et al. 1995) wrapped into a Python script. In brief, the pipeline automatically flags the data for RFI using a clipping method after filtering the data in both the frequency and time domain. After primary bandpass calibration, it iteratively deconvolves the data with the CLEAN algorithm in order to apply a self-calibration, using CLEAN masks determined on the cube with decreasing clip levels. We then subtract the continuum in the visibility domain and apply the calibration solution to the visibilities to then invert the data after Hanning smoothing. We then iteratively clean the data cubes down to the rms noise in the cubes, using CLEAN masks determined by filtering the data cubes with Gaussian kernels and applying a clip level. We used a Robust weighting of  $r=0.4$ , and binned the data to a velocity resolution of  $12.3 \text{ km s}^{-1}$  (FWHM;  $6.0 \text{ km s}^{-1}$  channels) after Hanning smoothing.

For each cube we then created H I total flux maps by smoothing the images to  $2 \times$  the beam size, masking any pixel below  $3\sigma$ , applying the mask to the unsmoothed cubes, and then summing along the velocity axis. We calculate H I column densities assuming optically thin H I gas that fills the WSRT beam, and also produce H I moment 1 velocity maps from cubes masked at  $3\sigma$ . We measure the H I flux by applying a mask based on the smoothed moment 0 map to cubes corrected for primary beam attenuation, and then extracting and fitting 1D spatially integrated H I profiles. These fluxes are reported in Table 1.

## 4 RESULTS

Figure 3 shows the ALFALFA moment 0 map of the central  $\sim 20 \text{ deg}^2$  of the regridded cube. At 25 Mpc, this image covers  $\sim 2 \times 2 \text{ Mpc}$  on the sky. The NGC 3227 and NGC 3190 groups are visible to the southeast and northwest of the center of the image, and are shown in greater detail in Figures 4 and 6 respectively. The H I plumes associated with NGC 3227 and the large feature in the NGC 3190 group extend to similar scales as the groups themselves. Indeed, Makarov & Karachentsev (2011) estimate the harmonic radii of the NGC 3227 and NGC 3190 groups to be 125 kpc and 276 kpc respectively (at  $D=25 \text{ Mpc}$ ), significantly less than the projected length of the structures discussed below. The large extent of these H I features is the main result of this paper. Here we describe the properties and extent of the features in the NGC 3227 and NGC 3190



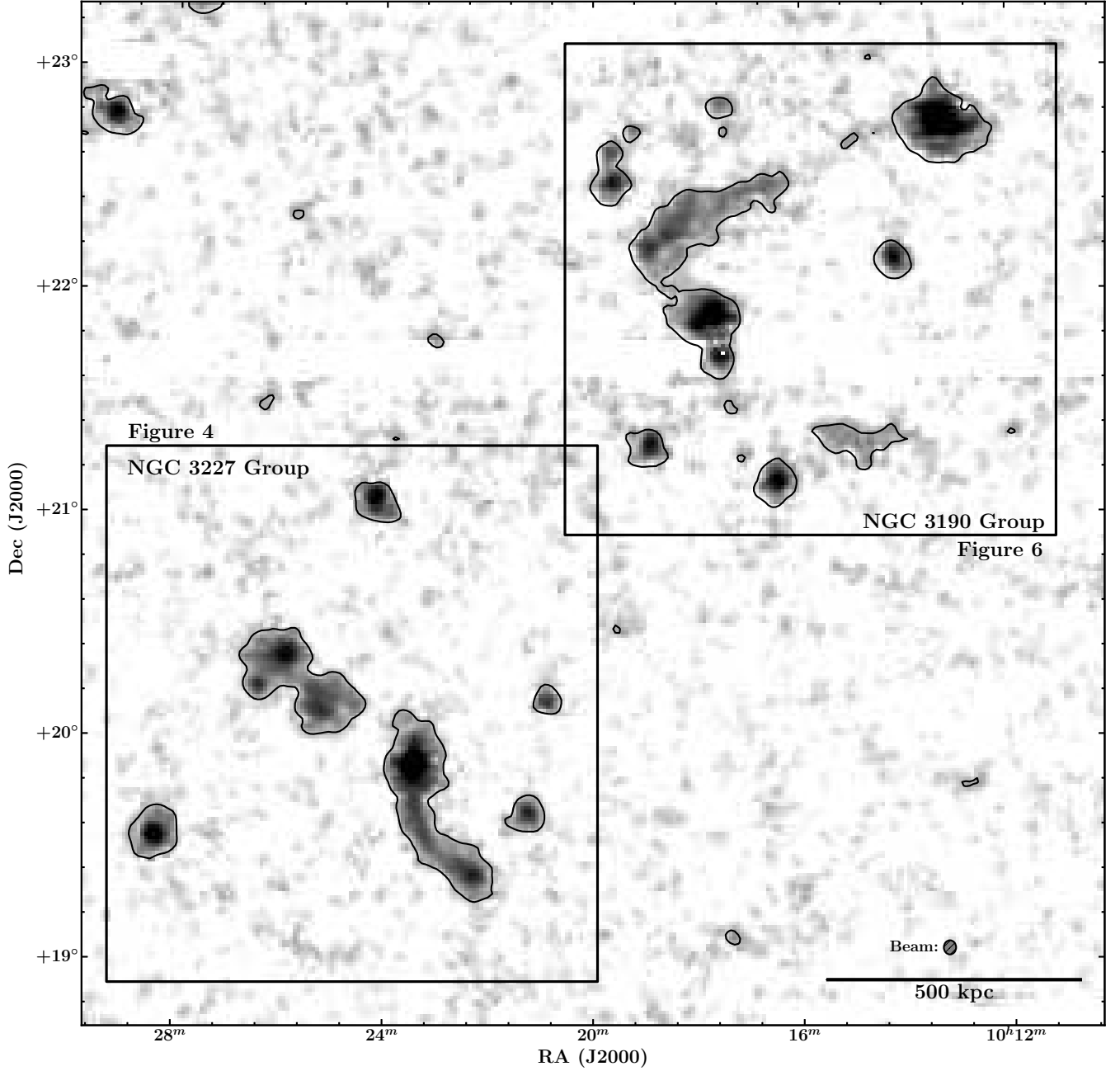


**Figure 3.**  $\sim 2 \times 2$  Mpc ALFALFA H I moment 0 map of the region containing the NGC 3190 and NGC 3227 groups, from 911 to 1722 km s<sup>-1</sup>, with boxes indicating the approximate locations of the two groups, and black contours denoting emission  $4\sigma$  above the average rms noise of the image. This map reveals that the H I features in the groups approach the scale of the group. The extent of the features was previously undetected in WSRT and VLA synthesis observations because of their lower sensitivity, and restriction to a  $\sim 0.5$  degree primary beam. A few strips with no emission (especially around  $\delta \sim 21^d + 38^m$ ) have been heavily masked due to significant RFI.

groups in sections 4.1 and 4.2, and then discuss the mass of cold intragroup gas in section 4.3.

#### 4.1 Extended Tails in the NGC 3227 Group

Figure 4 shows the ALFALFA data for the NGC 3227 Group, overlaid on an SDSS r-band image created with Montage. The bottom and side panels show RA-velocity and Dec-velocity views of the group, with black vertical and horizontal bars indicate the ALFALFA velocity width at the 50%

flux level for detected galaxies. A dashed thick black circle indicates the region imaged by Mundell et al. (1995), who report the detection of two H I plumes (labelled H I<sub>North</sub> and H I<sub>South</sub> in Figure 4) extending 51 and 116 kpc to the north and south of NGC 3227 in the center of the NGC 3227 group. However, the primary beam of the VLA at 1420 MHz (the effective field of view of the interferometer) is only  $\sim 35'$ . Thus, while, the ALFALFA data confirm the plumes detected in the high resolution VLA maps, they find that the plumes extend far beyond the VLA primary beam to  $\sim 10$  and  $\sim 40$

arcminutes (73 and 291 kpc at 25 Mpc). They also reveal the presence of a previously unreported feature stretching 0.9 degrees to the NE (labelled  $\text{HI}_{\text{NE}}$  in Figure 4), distinct from the other plumes.

All three H I appendages appear to have no detectable stellar counterparts at the surface brightness limit of SDSS ( $\sim 25$  mags  $\text{asec}^{-2}$ ); optically detected galaxies of known redshift (i.e. of  $m_g < 17.7$ ) are indicated with open diamonds, color coded by their velocity to match the scale in Figure 1. While there are several reasonably bright optical sources in this region, none of them are clearly associated with the H I features.

#### 4.1.1 The Southern H I Plume ( $\text{HI}_{\text{South}}$ )

The H I plume extending to the south of NGC 3227 shows excellent agreement with the [Mundell et al. \(1995\)](#) maps within the region imaged by the VLA. Both data sets show that the plume (which we will refer to as  $\text{HI}_{\text{South}}$ ) rises steeply in velocity from  $\sim 1200$   $\text{km s}^{-1}$  to  $\sim 1300$   $\text{km s}^{-1}$  moving south away from NGC 3227. However, the feature extends  $\sim 28'$  beyond the region covered by the VLA, continuing to rise in velocity, and decrease in projected column density.  $\sim 17'$  from NGC 3226/7, it bends west and begins to decrease in velocity from  $\sim 1320$  to  $\sim 1270$   $\text{km s}^{-1}$ . As shown in the PV panels in Figure 4, the end of the plume shows a marked increase in projected column density, and the velocity dispersion of the tail appears to decrease significantly moving south from NGC 3227. However, the significantly higher resolution WSRT observations of the end of the plume, shown in panels c and d of Figure 5, show a messy, extended distribution, inconsistent with any suggestion of a “dark” or tidal dwarf galaxy (TDG). Indeed, the higher column density emission traces the ALFALFA data well, and has clear elongated, tail like morphology. The column density peaks at  $2.3 \times 10^{20}$   $\text{atoms cm}^{-2}$  (for a beam of  $14'' \times 47''$ ), but there is no associated stellar emission at the detection limits of SDSS. There is a low surface brightness galaxy at  $10^{\text{h}}22^{\text{m}}53.2^{\text{s}} + 19^{\circ}34'36''$  without a measured redshift, but there is no associated H I in the higher resolution WSRT images. The bright elliptical galaxy at  $10^{\text{h}}22^{\text{m}}37.7^{\text{s}} + 19^{\circ}23'49''$  has a measured redshift of 11,792  $\text{km s}^{-1}$ .

We note that NGC 3213 is  $\sim 22'$  ( $\sim 160$  kpc) from the end of  $\text{HI}_{\text{South}}$ , has a similar recessional velocity (see the RA-velocity plot in Figure 4), and appears to show some extended H I emission at low SNR; however, our data do not have the sensitivity to determine if it is related to this southern plume. Thus, the H I distribution mapped here is consistent with the properties of a tidal tail associated with the merging pair NGC 3226/7, but we cannot completely rule out the rather unlikely possibility that  $\text{HI}_{\text{South}}$  is instead an H I bridge.

#### 4.1.2 The Northern H I Plume ( $\text{HI}_{\text{North}}$ )

The northern plume reported in [Mundell et al. \(1995\)](#) also is consistent with the ALFALFA data, but is blended with the emission from the TDG identified in [Mundell et al. \(2004\)](#) and NGC 3227, in Figure 4. While it appears to spatially connect with the northeastern feature ( $\text{HI}_{\text{NE}}$ , discussed below), the two tails are well separated in velocity space, as

demonstrated in the PV diagrams in Figure 4. The northern structure increases in velocity from 1300 to 1400  $\text{km s}^{-1}$ , as one moves away from NGC 3226/7 to a projected linear separation of  $15'$  (compared with  $\text{HI}_{\text{NE}}$  (section 4.1.3), which approaches NGC 3226/7 at a recessional velocity of 1240  $\text{km s}^{-1}$ ).

[Appleton et al. \(2014\)](#) use Spitzer IRAC observations together with the VLA H I data to connect this northern structure to the elliptical galaxy NGC 3226, suggesting that the gas is infalling onto NGC 3226. We note that it shows a significantly wider velocity dispersion ( $\sim 50$   $\text{km s}^{-1}$ ), and steeper velocity gradient than  $\text{HI}_{\text{South}}$ , and that there are suggestions of significant substructure at lower SNR. There are two blue, fuzzy galaxies of moderate magnitude (AGC 718681 with  $M_r = -17.3$  and AGC 718673 with  $M_r = -16.1$  at 25 Mpc) that fall within this plume’s H I contours, but both objects have recessional velocities that fall below that of the detected H I (1151  $\text{km s}^{-1}$  and 1166  $\text{km s}^{-1}$  respectively). The compact dwarf AGC 739353 near NGC 3226 has a recessional velocity of 1338  $\text{km s}^{-1}$ , somewhat higher than  $\text{HI}_{\text{North}}$ . Further modelling will be necessary to confirm the origins of this feature (and if, in fact it is a tidal tail, a tidal bridge, or something else).

#### 4.1.3 The Northeastern Feature ( $\text{HI}_{\text{NE}}$ )

Figure 4 also shows a bright H I feature extending 0.9 degrees to the northeast of NGC 3226/7. The feature is somewhat more massive than  $\text{HI}_{\text{South}}$ , but has a clumpier gas distribution, higher velocity dispersion, and more complicated velocity field. The nature of the feature’s connection to NGC 3226/7 was not immediately clear, since it is not connected at the column density sensitivity of our data. However, emission detected at  $2.5\sigma$  in at least 3 neighbouring beams leads away from NGC 3226/7 at around 1230  $\text{km s}^{-1}$  (most easily seen in the PV diagrams), forming a smooth arc with the rest of the NE tail. This feature shows two primary projected density peaks in the ALFALFA data, one roughly associated with the velocity minimum, and the other near the end of the tail. The WSRT observations, shown in Figure 5, resolve these peaks into several clumps, revealing complicated structure in the high column density emission. The SW clump appears messy with two or more density peaks, and the velocity field suggests it may contain significant substructure. Some of the emission extends in the NE-SW direction, while the emission at higher velocity is elongated in the EW direction. The NE structure appears as a single clump with a peak column density of  $3.9 \times 10^{20}$   $\text{cm}^{-2}$  in the WSRT data (assuming the flux fills the  $13'' \times 41''$  beam integrated over the width of the source), but does not appear to show coherent velocity structure.

The disordered morphology at high column density, and the smooth, correlated nature of the structures in the ALFALFA data point to a tidal connection between NGC 3226/7 and this NE structure. However, detailed modelling will be required to understand the full history of this feature, which may be the product of several interactions within the group.

The entire structure shows no stellar emission in SDSS imaging. There are 3 optical galaxies with measured redshifts in the nearby vicinity. AGC 718719 is fairly small and blue, and appears in projection near NGC 3226/7. How-

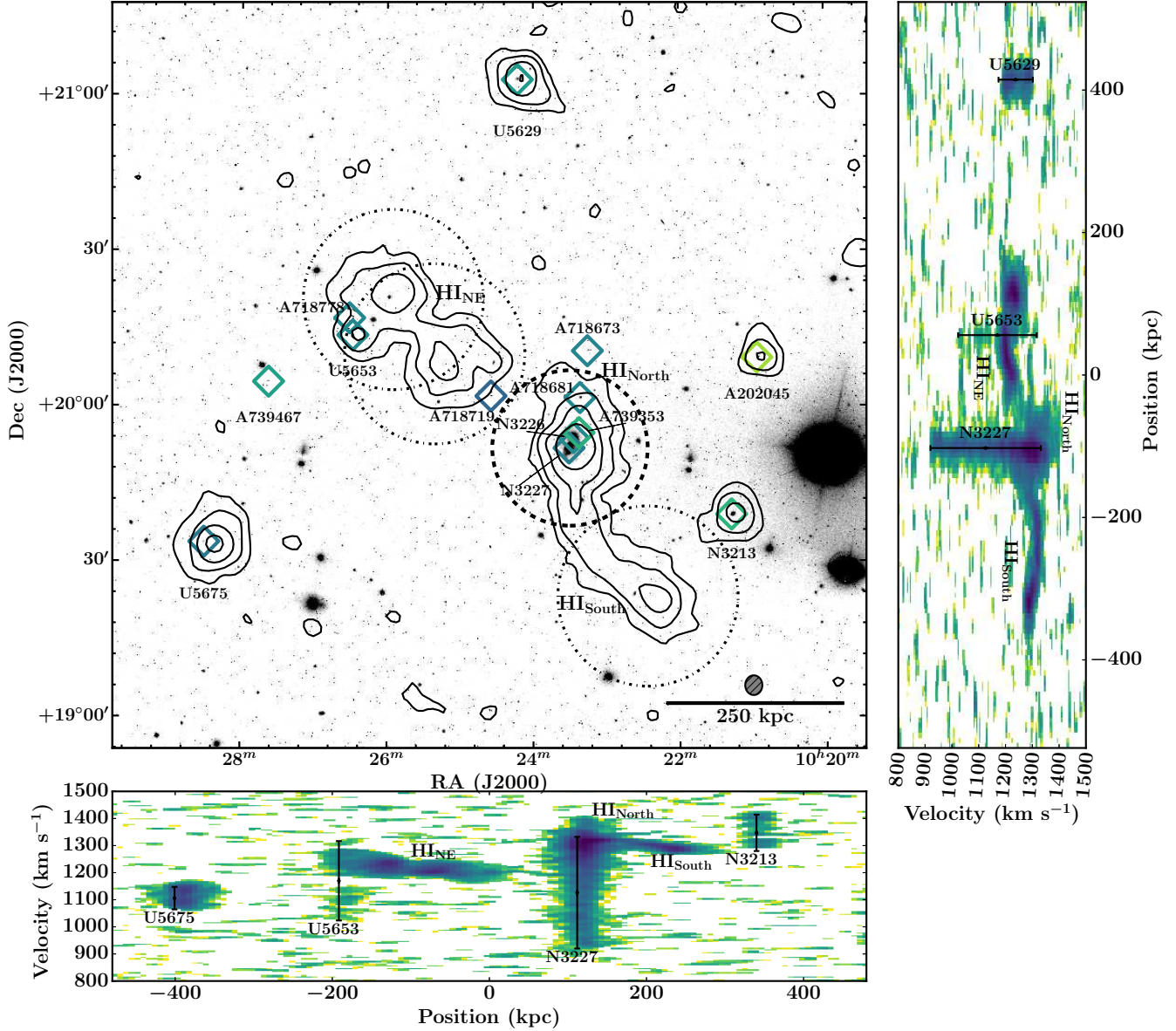


**Figure 4.** ALFALFA moment 0 contours (summed over 900 to 1500  $\text{km s}^{-1}$ ) overlaid on a SDSS r-band optical image of the NGC 3227 group, demonstrating the large extent of the H I features relative to the optical emission from the merging pair NGC 3226/7 (near the center of the image). Contour levels are spaced logarithmically at 1.2, 2.4, 4.8, 9.6, and  $19.2 \times 10^{18}$  atoms  $\text{cm}^{-2}$  (assuming the H I uniformly fills the ALFA beam of  $3.3' \times 3.8'$ ). The lowest contour level is  $4\sigma$  above the rms noise. The thick dashed circle indicates the region mapped in higher resolution VLA imaging by [Mundell et al. \(1995\)](#), showing the need for wide field mapping for a full understanding of this system. The thinner dash dotted circles show the field of view of the WSRT observations shown in Figure 5. Optical galaxies with known redshifts between 700 and 1700  $\text{km s}^{-1}$  are marked with open diamonds, coloured by their recessional velocity to match the colour scale from Figure 1. Catalog designations AGC, UGC, and NGC are abbreviated by their first initial. The ALFA beam is represented by a hashed circle in the lower right. Right and Bottom: ALFALFA position-velocity diagram summing the H I emission across the image from 10:27:30 to 10:21:45 in RA and from 19:00:00 to 20:40:00 in Dec respectively (the ranges are selected to minimize confusion and highlight the H I plumes in the diagrams). Black vertical and horizontal bars indicate the ALFALFA velocity width at the 50% flux level for detected galaxies in the region. The diagrams show the coherence of the plumes in velocity space, and the separation in velocity of  $\text{HI}_{\text{NE}}$  at  $\sim 1200 \text{ km s}^{-1}$  and  $\text{HI}_{\text{North}}$  at  $\sim 1400 \text{ km s}^{-1}$ .

ever, with a recessional velocity of  $1028 \text{ km s}^{-1}$  it appears to be unrelated to the details of the tail. AGC 718778 ( $v_{\text{helio}} = 1163 \text{ km s}^{-1}$ ) is a low surface brightness dwarf located near the northeastern end of the tail, and at a more similar velocity to the tail, but is still at a lower recessional velocity than the detected gas. UGC 5653 is an edge on spiral with a clear dust lane located in the vicinity, but to the

south of  $\text{HI}_{\text{NE}}$ . While some of the emission from UGC 5653 is blended with  $\text{HI}_{\text{NE}}$ , its central recessional velocity is lower than bulk of the nearby emission from  $\text{HI}_{\text{NE}}$  ( $1170 \text{ km s}^{-1}$  when separated from the other emission). It is possible that  $\text{HI}_{\text{NE}}$  is, in fact, a bridge between UGC 5653 and NGC 3227, however the WSRT observations do not indicate a clear connection between the H I in UGC 5653 and  $\text{HI}_{\text{NE}}$ , and the



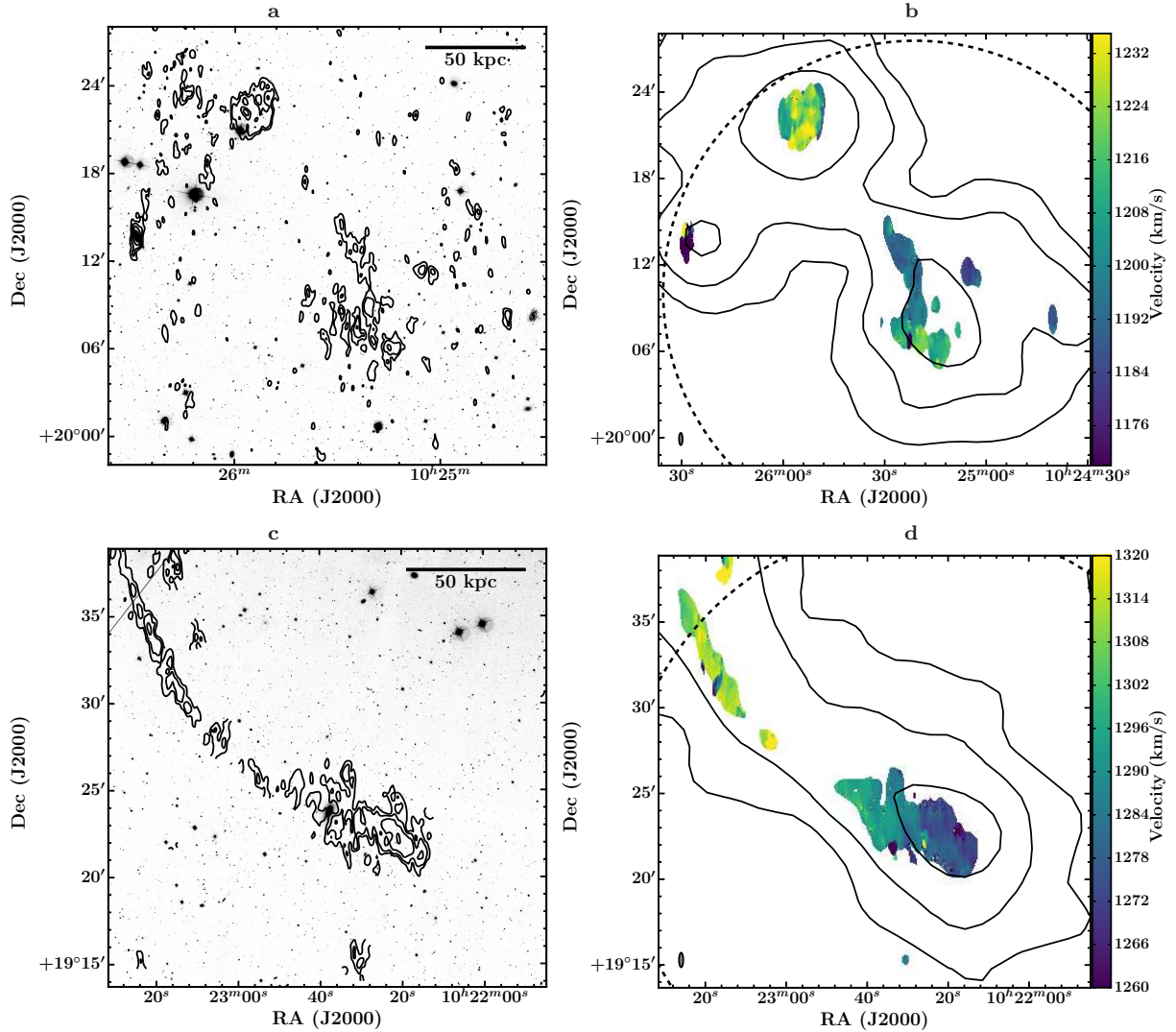


**Figure 5.** Left: High resolution WSRT synthesis imaging of the ends of the Northeastern (HI<sub>NE</sub>) and Southern (HI<sub>South</sub>) H I features associated with NGC 3227, showing messy, apparently tidal morphology in the higher column density gas. Panels a and c show WSRT H I column density contours at 3.5, 7, 14, 28, and  $56 \times 10^{19}$  atoms  $\text{cm}^{-2}$  (assuming the H I uniformly fills the beam of  $14'' \times 47''$ ) of HI<sub>NE</sub> and HI<sub>South</sub> respectively, overlaid on g-band images from SDSS created with Montage. Panels b and d show WSRT moment 1 maps of HI<sub>NE</sub> and HI<sub>South</sub> respectively, with ALFALFA flux density contours from Figure 4 overlaid in black. The WSRT observations match well with the lower resolution ALFALFA observations, and both features show coherent velocity structure. The FWHM of the WSRT primary beam is indicated by black dashed circles; significant primary beam corrections are necessary to estimate the flux of the entire features. The WSRT beam is indicated by a small grey circle in the lower left corner of panels b and d.

geometry seems rather unfavourable. Further, without measured primary distances, velocity crowding from infall requires that these sources be interpreted with caution since there is a small chance that they are simply projected to a similar region of phase space. However, we do note that the 6 objects detected without any H I in this subgroup (besides NGC 3226; listed in the bottom of Table 1) are all in close proximity to HI<sub>NE</sub> or HI<sub>North</sub> discussed above, and have somewhat similar optical colours and morphologies. All other objects brighter than  $m_g = 17.7$  have detected H I in ALFALFA.

The moment 0 map also reveals suggestive tidal features at low SNR extending to the southwest of the NE plume toward the low surface brightness dwarf galaxy UGC 5675. However, deeper observations would be necessary to put this low SNR suggestion on firmer footing. Understanding the

origins of the three main features detected here will require detailed dynamical modelling.

## 4.2 Extended Tails in the NGC 3190 Group

Located approximately 1 Mpc to the NW of the NGC 3227 group, the NGC 3190 group is the other primary overdensity in the NBG 21-6 region. Like the NGC 3227 group, the NGC 3190 group is known to exhibit extended H I without apparent associated stellar emission. Specifically, using a deep 6x12h pointing with WSRT, [Serra et al. \(2013\)](#) reported the detection of a large H I feature (which they refer to as the northern tail, T<sub>N</sub>) near the center of the group, extending  $\sim 20'$  (220 kpc) to the northwest of HCG 44, and optically dark down to  $\mu_g = 28.5$  mags  $\text{arcsec}^{-2}$  (in deep CFHT



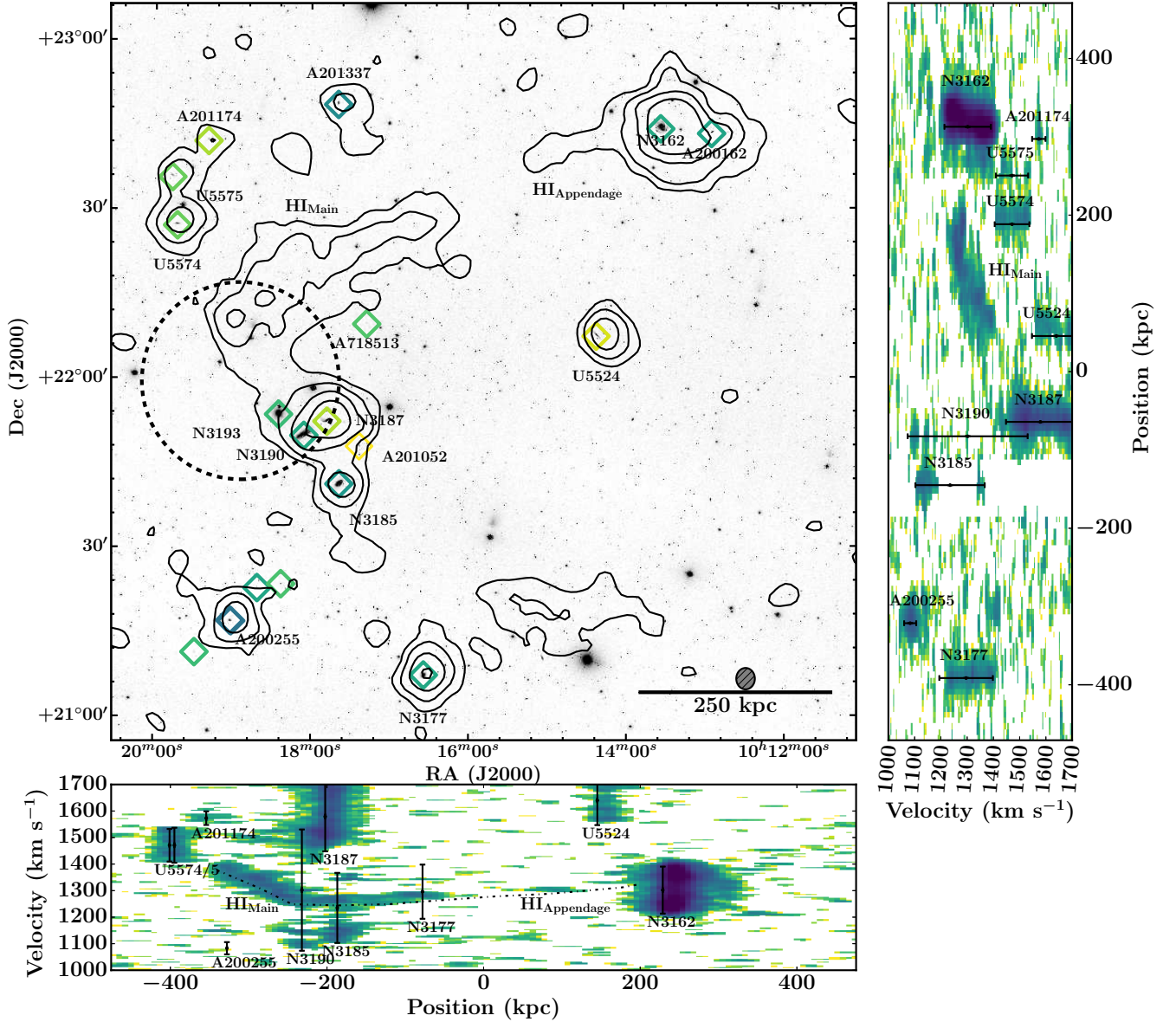


**Figure 6.** ALFALFA imaging of the central region of the NGC 3190 subgroup overlaid on an SDSS r-band optical image, showing the extended dark feature to the north of HCG 44, and the likely connection to NGC 3162. Optical galaxies with measured redshifts are indicated by open diamonds as in Figure 4. The ALFALFA moment 0 contour levels are spaced logarithmically at 2, 6, 18, and  $54 \times 10^{18}$  atoms  $\text{cm}^{-2}$  (assuming the H I uniformly fills the ALFA beam of  $3.3' \times 3.8'$ ). The lowest contour level is  $4\sigma$  above the rms noise. The black dashed circle indicates the FWHM of the WSRT primary beam from Serra et al. (2013). Note that the entire northern tail appears optically dark at the detection limits of SDSS. Right and Bottom: ALFALFA PV diagrams summing the H I emission across the image from  $10^{\text{h}} 12^{\text{m}}$  to  $10^{\text{h}} 20^{\text{m}}$  in RA and from  $21^{\circ} 30'$  to  $23^{\circ}$  in Dec respectively (the ranges are selected to minimize confusion in the diagrams). Note that NGC 3185 is missing significant emission between  $v \sim 1200$ – $1300$   $\text{km s}^{-1}$  due to RFI masking, so the entirety of the main H I tail is visible in the bottom PV diagram. The emission from HI<sub>Main</sub> and HI<sub>Appendage</sub> are underscored by a dashed dotted line, showing that they align well in both position and velocity.

imaging). They further note the detection of HIPASS emission beyond the edge of the WSRT primary beam, which might extend the tail to  $\sim 300$  kpc, and the detection of a small cloud ( $C_s$ ) to the east of HCG 44 and the south of the main H I feature. They suggest that the large H I feature originated due to tidal stripping, and suggest that it may have originated from an interaction between NGC 3190 and NGC 3187, or from an interaction between NGC 3162 and the members of the compact group during a close flyby.

Like in the NGC 3227 group, ALFALFA finds that this previously detected H I feature extends to the group scale, well beyond the region previously studied, and finds evidence of additional extended H I structures. Figure 6 shows ALFALFA H I column density contours overlaid on a Montage SDSS g-band mosaic of the NGC 3190 group. The primary beam from Serra et al. (2013) is shown as a black dashed circle. The ALFALFA observations, which have an effective integration time of 40 seconds per beam, are sensitive to low

column density structure across the entire group, and show that full extent of the primary H I structure. This feature, which we will refer to as  $\text{HI}_{\text{Main}}$  hereafter, contains all of  $T_N$  and the suggestive HIPASS emission, and more, covering  $\sim 45'$  (330 kpc) across the sky. The feature shows significant substructure, which is confirmed in a recent, deep pointing with KAT-7, and discussed in detail in Hess et al., submitted.

The ALFALFA data further show a low column density extension stretching SE from NGC 3162 in the direction of  $\text{HI}_{\text{Main}}$ . This appendage ( $\text{HI}_{\text{Appendage}}$ ) is relatively low signal to noise, but is detected at  $>2.5\sigma$  in 6 contiguous beams, and has a narrow ( $W_{50}=31 \text{ km s}^{-1}$ ), but coherent structure in velocity space. Moreover, it is not simply a sidelobe of NGC 3162, since it extends  $\sim 30'$  from the center of NGC 3162 (the peak of the first ALFA sidelobe is at  $\sim 5'$ ). The emission from the NGC 3162 extension does not connect directly to  $\text{HI}_{\text{Main}}$  at the sensitivity of the ALFALFA data, however, Figure 6 demonstrates that they are well aligned both spatially and in velocity space, strongly suggesting that  $\text{HI}_{\text{Main}}$  is, in fact connected to NGC 3162. The apparent connection of the H I features means that the entire structure is nearly 1.4 degrees (610 kpc) long.

Several other weaker pieces of evidence fit with the interpretation that  $\text{HI}_{\text{Main}}$  is associated with NGC 3162. The mass budget, presented below in section 4.3, argues for the reality of the connection to NGC 3162, since the tail contains 20% of the H I mass of NGC 3162, but at least 40% of the H I mass of any of the sources in HCG 44. Additionally, NGC 3162 shows some sign of the presence of a forward tail encompassing the smaller spiral AGC 200162, and the gas in the full H I structure appears to spread out spatially as it moves away from NGC 3162, possibly consistent with gas spreading as a function of time after leaving NGC 3162. However, we note that the velocity dispersion smoothly increases from  $\sim 20 \text{ km s}^{-1}$  to  $\sim 60 \text{ km s}^{-1}$  moving away from NGC 3162, which seems to suggest energy input from HCG 44.

Indeed, since  $\text{HI}_{\text{Main}}$  lies within the disk velocities of both NGC 3162 and NGC 3190, it is reasonable to assume that the feature is related to both sources. However, The connection between the giant H I feature and the galaxies of HCG 44 is less clear. The moment 0 contours in Figure 6 show a low column density bridge between the brightest parts of the tail and HCG 44. However, when examined in velocity space, the ALFALFA data hint that the extended H I may be composed of at least two superimposed kinematic features. Figure 7 presents the region surrounding  $\text{HI}_{\text{Main}}$ , masked to contain just the emission clearly associated with the extended H I structures. The blue-green contours show the H I emission associated with  $\text{HI}_{\text{Main}}$  and  $\text{HI}_{\text{Appendage}}$  demonstrating that together they extend nearly continuously from NGC 3162 toward a point  $\sim 20'$  north of HCG 44, bending through velocity space from  $\sim 1300 \text{ km s}^{-1}$  near NGC 3162 down to  $\sim 1250 \text{ km s}^{-1}$ , and then receding to  $\sim 1400 \text{ km s}^{-1}$ . Near the SE end of  $\text{HI}_{\text{Main}}$  the H I appears to reach south from the main feature toward NGC 3190, potentially suggesting a connection between  $\text{HI}_{\text{Main}}$  and the compact group. However, combination of the ALFALFA data with the WSRT data from Serra et al. (2013) and with recently obtained KAT-7 data (Hess et al., submitted) shows no strong evidence that  $\text{HI}_{\text{Main}}$  is connected to HCG 44 in the deeper cube.

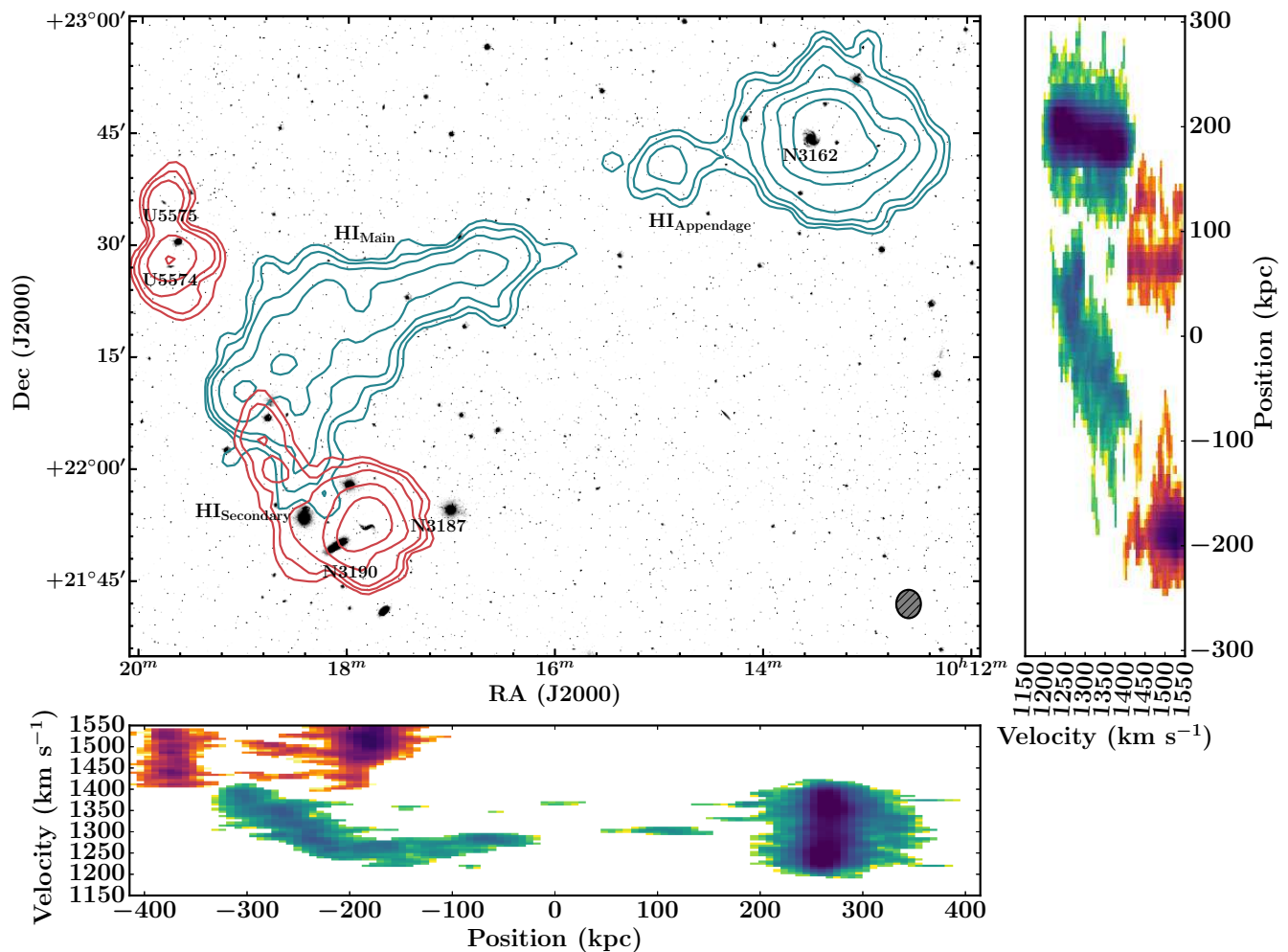
The red contours in Figure 7 show H I emission summed over velocities above  $1400 \text{ km s}^{-1}$ . These reveal a potential second, low column density, low signal to noise structure, hereafter  $\text{HI}_{\text{Secondary}}$ , visible at higher velocities ( $\sim 1500 \text{ km s}^{-1}$ ). The structure extends east from NGC 3187 to encompass the cloud dubbed  $C_S$  in Serra et al. (2013), and then north toward UGC 5574, UGC 5575, and AGC 201174, at matching recessional velocities. This suggestion, however, is tentative, since the structure is detected at low significance (the significance of this structure in Figure 7 is potentially exaggerated by the superposition of signal from multiple low significance features). The combined ALFALFA, WSRT, and KAT-7 data (Hess et al., submitted) also shows a compact H I cloud at the location of the northern peak in the red contours in Figure 7, but do not show clear emission connecting it to  $C_S$  or NGC 3187. Thus, much of the extent of this structure is likely a result of beam smearing and artefacts in the ALFALFA data.

Figure 6 also shows the apparent detection of an extended feature around  $10^h 15^m +21^\circ 20'$ . Analysis of the ALFALFA spectrum at this position shows significant baseline fluctuations, consistent with low level RFI not masked by our other algorithms. Similarly, Figure 6 also shows the suggestion of a southern extension off NGC 3185, however, this extension is in the region of the cube with low weights due to significant RFI. Thus, further observations of these regions will be necessary to know if there is any real H I emission to the south and southeast of HCG 44.

### 4.3 The H I mass budget in the NGC 3190 and NGC 3227 intragroup medium

The extended features in both the NGC 3190 and NGC 3227 groups contain a significant fraction of the total H I in the group. Tables 1 and 2 list the fluxes and H I masses for all sources detected by ALFALFA in the NGC 3227 and NGC 3190 groups respectively, assuming a common distance of 25 Mpc (note that under this assumption, the NGC 3190 group contains  $1.5\times$  the H I mass of NGC 3227 group). Column 10 gives the full breakdown of H I in each group, listing the percentage of H I in each feature relative to the sum of each subgroup. The dark plumes in the NGC 3227 group ( $\text{HI}_{\text{North}}$ ,  $\text{HI}_{\text{South}}$ , and  $\text{HI}_{\text{NE}}$ ) have a combined log H I mass of 9.47, 40% of the total H I in the group, and 53% of the gas associated with NGC 3226/7. Only slightly less massive,  $\text{HI}_{\text{Main}}$  in the NGC 3190 group has a log H I mass of 9.05, making up 10% of the total group H I mass. However, 40% of the H I mass of the NGC 3190 group is contained in NGC 3162;  $\text{HI}_{\text{Main}}$  is nearly 30% of the combined H I mass of the galaxies in HCG 44. For comparison, the Leo Ring makes up 24% of the  $M_{\text{H I}}$  in the M96 group, and tidal plumes in the Leo Triplet constitute 14% of the H I mass in the M66 group (Stierwalt et al. 2009).

Comparisons to synthesis imaging can give a sense of the amount of low surface density gas in these intragroup features, but direct comparison is difficult due to significant differences in the data and the subsequent analysis. Tables 1 and 2 give synthesis measurements where available. WSRT observations recover 94% of the flux in  $\text{HI}_{\text{NE}}$ , and 74% of the flux in  $\text{HI}_{\text{South}}$  in the NGC 3227 group. However, the large extent of the dark H I features necessitates large primary beam corrections for the portions of



**Figure 7.** ALFALFA moment 0 H I contours, masked to highlight the primary H I features in the NGC 3190 group, overlaid on SDSS g-band optical images, with PV diagrams as in Figure 6. The blue-green contours and blue to green coloured emission in the PV diagrams outline the entire main feature (HI<sub>Main</sub>), which is visible at velocities below 1400 km s<sup>-1</sup>, and appears to be associated with NGC 3162. The red contours and red to magenta coloured emission at velocities above 1400 km s<sup>-1</sup> show the suggestion of a secondary feature (HI<sub>Secondary</sub>) at higher velocity, which may suggesting a connection between NGC 3187 and UGC 5574, but this feature is only partially confirmed in deeper data (Hess et al., submitted). Contour levels are spaced logarithmically at 6, 12, 24, 48 96, and 192×10<sup>17</sup> atoms cm<sup>-2</sup> (assuming the H I uniformly fills the ALFA beam).

the sources near the edge of the beam, which means these results should not be over interpreted. For example, WSRT measures the flux of HI<sub>South</sub> to be 5.1±0.2 Jy km s<sup>-1</sup>. However, if one only measures the flux outside the Mundell et al. (1995) observation, and combines it with the Mundell et al. (1995) VLA flux of 2.42 Jy km s<sup>-1</sup>, the summed synthesis observations give a flux of 6.0 Jy km s<sup>-1</sup>. It is also worth noting that Mundell et al. (1995) measured a larger flux for HI<sub>North</sub> than ALFALFA. However, the flux for HI<sub>North</sub> is significantly blended with that of NGC 3227 in the ALFALFA data, so the artificially low flux of HI<sub>North</sub> is likely due to conservative deblending. A reasonable deduction from these data is that a significant portion of the flux in the NGC 3227 subgroup is coming from the higher column density gas detected in synthesis observations.

ALFALFA detects fluxes significantly higher than those reported from WSRT in Serra et al. (2013), with the WSRT observations recovering between 43% and 88% of the AL-

FALFA flux for galaxies in HCG 44. However, it is worth noting that the ALFALFA fluxes for NGC 3187 and NGC 3190 individually contain significant uncertainty, since their emission is blended in the ALFALFA cubes. It is also important to note that the flux of NGC 3185 is likely significantly affected by RFI, in spite of care during source parameter extraction to mitigate this effect. The range in recovered fluxes may suggest that HCG 44 is surrounded by significant lower column density gas.

Notably, ALFALFA detects the entirety of the H I tail reported in Serra et al. (2013), and is unaffected by beam attenuation. Serra et al. (2013) report a total tail log H I mass of 8.71 after including HIPASS emission detected in re-reduced cubes. ALFALFA measures a total log H I tail mass of 9.05±0.03, 2.2× higher than the WSRT+HIPASS measurement, significantly more than their stated typical flux uncertainties of 10-20%.



## 5 DISCUSSION

The ALFALFA maps of the NBG 21-6 region underscore the need for sensitive, wide field surveys to obtain a complete understanding of ongoing galaxy evolution in groups. Specifically, the detection of H I tails and bridges on scales larger than the group virial radius suggests strong ties between the evolution of galaxies in this region, and their group environment. Here we discuss the regional context of the sources presented above as evidence of ongoing hierarchical galaxy assembly.

### 5.1 HCG 44 in the Context of the NGC 3190 Group

Previous studies of the H I in the NGC 3190 group have focused on understanding the evolutionary state of HCG 44 in the context of other compact groups. Verdes-Montenegro et al. (2001) propose an evolutionary sequence where a compact group's H I deficiency (Haynes et al. 1984) increases with time due to multiple tidal interactions, and find the H I deficiency of the members of HCG 44 to be high relative to other compact groups.<sup>1</sup> Similarly, Borthakur et al. (2010) and Borthakur et al. (2015) use the Green Bank Telescope to find evidence of diffuse H I in compact groups, but find that most of the gas in a 180×180 kpc (25'×25') region surrounding the central galaxies of HCG 44 originates in high column density, disk-like structures. However, the apparent connection between NGC 3162 and HCG 44 in the ALFALFA data suggests that HCG 44 is best understood in the context of the entire NGC 3190 group.

Using H I synthesis maps, Serra et al. (2013) propose that the large H I feature originated due to tidal stripping, and suggest two specific origins: 1) within the compact group due to an interaction between NGC 3190 and NGC 3187, or 2) from an interaction between NGC 3162 and the members of the compact group during a close flyby. In the context of the entire group, the ALFALFA data strongly favour the second hypothesis.

Serra et al. (2013) suggest that if the H I feature originated in HCG 44, it could at least partially explain the observed H I deficiency. However, NGC 3162 dominates the H I mass budget of the NGC 3190 group, with more than 150% of the H I mass contained in NGC 3185, NGC 3187, and NGC 3190 combined. While a highly disruptive event could remove ~50% of the gas from e.g., NGC 3187, tidal forces should more easily remove ~20% of the gas from the outskirts of an H I-rich source like NGC 3162. Moreover, even after including the entire mass of H I<sub>Main</sub>, HCG 44 is still H I deficient by more than a factor of six. This, suggests the members of HCG 44 were likely gas poor prior to an interaction with NGC 3162, which would make it even more difficult to remove the remaining, more tightly bound gas.

<sup>1</sup> Verdes-Montenegro et al. (2001) measure the H I deficiency of NGC 3185 and 3190 to be +1.0 (10% of the expected gas), and the H I deficiency of NGC 3187 to be +0.4 (40% of the expected gas). Serra et al. (2013) get values a factor of 2 more deficient using the relations of Toribio et al. (2011), but we note that this difference can be explained by a typo swapping radius and diameter in the Toribio et al. (2011) relations.

Indeed, the potential detection of separate H I features like H I<sub>Secondary</sub> is consistent with the idea that the group has experienced other tidal interactions. Thus, the group context suggests a scenario where the interaction with NGC 3162 is only one of the interactions responsible for the removal of gas from the members of HCG 44, and that NGC 3162 is the primary source of the gas in the H I feature, potentially delivered on a first infall to the group.

Further, the scale of the interactions surrounding HCG 44 suggests interesting questions for studies of other compact groups. Since not all tidal interactions favour the creation of massive tidal tails, the existence of a ~600 kpc tail suggests that groups with less fortuitously aligned interactions on similar scales should exist. Studies like Walker et al. (2016) have found only weak correlations between the total H I in compact groups (as observed with GBT) and the properties of individual galaxies. However, the GBT has a 9' beam per pointing, and thus may miss significant group flux. In the case of HCG 44 ( $\log M_{\text{H I, total}} = 9.45$ ), the entire compact group fits within just a couple of GBT beam pointings, but neither the large H I tail ( $\log M_{\text{H I}} = 9.05$ ) nor NGC 3162 ( $\log M_{\text{H I}} = 9.65$ ) would be detected.

Thus, future wide-field surveys will be important for understanding the regions surrounding compact groups. While HCG 44 may be an extreme example, it presents a cautionary note that a full understanding of compact group scaling relations will likely require careful consideration of the surrounding ~1 Mpc via deep, wide field H I surveys.

### 5.2 Interactions in their Group Context

As discussed in section 4.1, the H I features in the NGC 3227 group suggest potential associations between NGC 3227 and other group members, including NGC 3213, UGC 5653, and the dwarf galaxies in close spatial proximity to the plumes. Similarly, the apparent connection between NGC 3162 and NGC 3190 makes it highly probable that they are at the same distance. In regions of the local universe with limited distance information, upcoming H I surveys will be an important tool for connecting sources with large distance uncertainties to those with primary distances. For example, a common way of determining group distances is to examine the Tully-Fisher relationship for the sources in the region (e.g. Figure 9 and the corresponding discussion in Section 5.3). However, stringent selection of galaxies for accurate distance determination (e.g. mostly edge on, similar Hubble types, etc.) often leaves too few sources for reliable distance determination, especially in compact groups where interactions may contribute to increased scatter in the relation. In these groups H I mapping coupled with stellar distance estimates from JWST will be an important source of reliable distances.

The potential tidal connection between sources separated by ~300 kpc has potential consequences for searches for tidal dwarf galaxies. Mundell et al. (2004) report a potential TDG candidate in close proximity to NGC 3226/7. While the plumes in the NGC 3227 group do not show clear evidence of TDGs further out at our current resolution, they do indicate that searches for tidal dwarf galaxies may require imaging at significant separations from their parent galaxies. For example, Lelli et al. (2015) analyse VLA observations of 6 merging systems containing TDGs at  $cz < 5000 \text{ km s}^{-1}$ . The



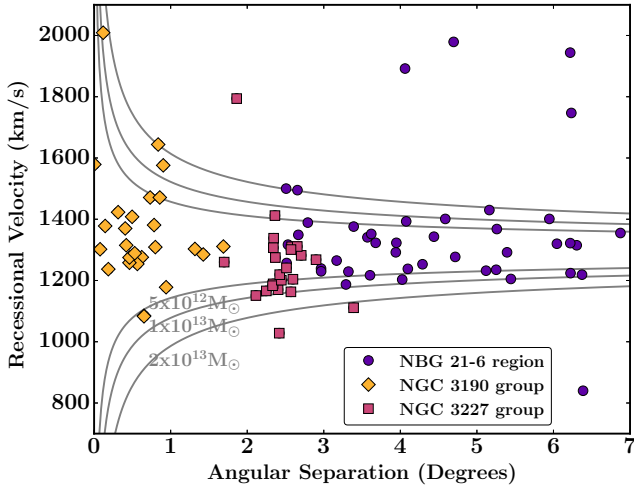


**Figure 8.** Angular separation on the sky versus recessional velocity for galaxies in the NBG 21-6 region, showing the dynamics of the larger region. Separations are measured from the center of HCG 44, which we take to be  $154.5 \pm 22$ . Green squares are the galaxies associated with the NGC 3227 group, and red diamonds are those associated with the NGC 3190 group. Blue circles are the other galaxies within 7 degrees of the center of HCG 44. At a distance of 25 Mpc, 7 degrees corresponds to  $\sim 3$  Mpc. Grey lines show simple caustic curves calculated using  $v = \sqrt{GM/2r}$  (see Section 5.3).

edges of the extended H I emission in the NGC 3227 group would still extend just beyond the VLA primary beam if it were at  $D=70$  Mpc ( $5000 \text{ km s}^{-1}$ ). More, numerical simulations predict differing numbers of potential tidal substrates per system (e.g. Bournaud & Duc 2006; Yang et al. 2014), so understanding the full scale of each interaction will be important in validating these predictions.

### 5.3 Hierarchical Structure Formation in the NBG 21-6 Region

The assembly of structures via mergers at all scales is a key prediction of hierarchical structure formation models. Thus, the discovery of two large tidal systems in relatively close proximity ( $\sim 1$  Mpc) motivates an examination of the surrounding region as a potential example of galaxy evolution on multiple scales.

As discussed in section 2, the grouping of galaxies in the NBG 21-6 region depends on the scale used in the grouping algorithm. However, the histogram in Figure 2 suggests a potential connection between galaxies in the broader region. Figure 8 plots the recessional velocities from Figure 2 as a function of angular separation from the center of HCG 44 (HCG 44 was selected as the dynamical center since it has the largest velocity dispersion of the region). The narrow velocity structure ( $\sigma \sim 115 \text{ km s}^{-1}$ ) over large angular scales suggests the region may be experiencing significant infall onto a larger, filamentary dark matter structure, though there are currently too few distance measurements to confirm this suggestion.

As a rough diagnostic tool, Figure 8 also shows simple caustic curves calculated using  $v = \sqrt{GM/2r}$  and assuming all sources are at a distance of 25 Mpc. The distribution of

sources in the region approximately match the velocity distribution expected for a sources moving in a potential of  $M = 2 \times 10^{13} M_{\odot}$ . Given the assumption of uniform distance and that this system is likely far out of equilibrium, these curves are at best suggestive. However, simple calculations of the dynamical mass of the NGC 3190 and NGC 3227 groups using the median mass calculation defined in Heisler et al. (1985) estimate masses of  $8.5$  and  $3.3 \times 10^{12} M_{\odot}$  respectively. We speculate that these estimates are consistent with a picture of the NGC 3190 and NGC 3227 groups as part of larger structure, falling toward the center of a larger common potential. Indeed, under the assumption that the two groups are moving toward each other, each with a velocity  $v = \sqrt{G \times 2 \times 10^{13} M_{\odot} / (2 \times 1 \text{ Mpc})} \approx 200 \text{ km s}^{-1}$ , the two systems will merge in  $\sim 3\text{--}4$  Gyr.

If all the galaxies in the region are actually part of the same structure and at a similar distance, we would expect them to follow the Tully-Fisher relation between their apparent magnitude and their H I velocity widths. Figure 9 shows the Tully-Fisher relation for sources contained within by the  $2 \times 10^{13} M_{\odot}$  caustics in this 6 Mpc diameter region. Optical magnitudes were taken from the NASA-Sloan Atlas<sup>1</sup> where available, since the NSA compensates for significant shredding issues in the SDSS pipeline magnitudes. They were converted to I-band magnitudes using the Lupton (2005) relations from the SDSS website, and corrected for internal and galactic extinction following Giovanelli et al. (1997a). NSA inclinations were checked by eyeball measurements, and any sources with  $(b/a)_{\text{NSA}} - (b/a)_{\text{eye}} > 0.2$  were removed. H I velocity widths from ALFALFA were converted to total widths following Giovanelli et al. (1997a), and all sources with  $i < 40$  were removed from the sample. Assuming all sources are the same distance and follow the Tully-Fisher relation from Giovanelli et al. (1997a), we estimate the best fit distance to be  $24.7 \pm 1.1$  Mpc using a single parameter orthogonal distance regression fit to the data.

The black line shows the I-band Tully-Fisher relation and error budget from Giovanelli et al. (1997a) and Giovanelli et al. (1997b), for a distance of 25 Mpc. The scatter around the relation is consistent with all sources at the same distance for the small number of sources available. However, while this result is consistent with the interpretation of (almost) all of the sources in the region being at the same distance, the lack of sources makes it impossible to strongly differentiate between that and significant distance scatter, since a source with  $W = 160 \text{ km s}^{-1}$  in the background by 5 Mpc, would only lie  $\sim 1\sigma$  off the relation. Thus, this calculation demonstrates the difficulty of using secondary relations to determine group distance. Significant source statistics to perform this kind of analysis will have to await next generation deep H I and optical surveys, and improved understanding of the faint end of the baryonic Tully Fisher relation.

The collective optical properties of galaxies in the NBG 21-6 region are consistent with expectations for galaxies experiencing significant large scale infall in a hierarchical formation model. Most of the sources in the NBG 21-6 region are dwarfs with a r-band absolute magnitude of  $M_r > -18$ . Most sources in the region are H I rich (ALFALFA detects

<sup>1</sup> <http://www.nsatlas.org/>

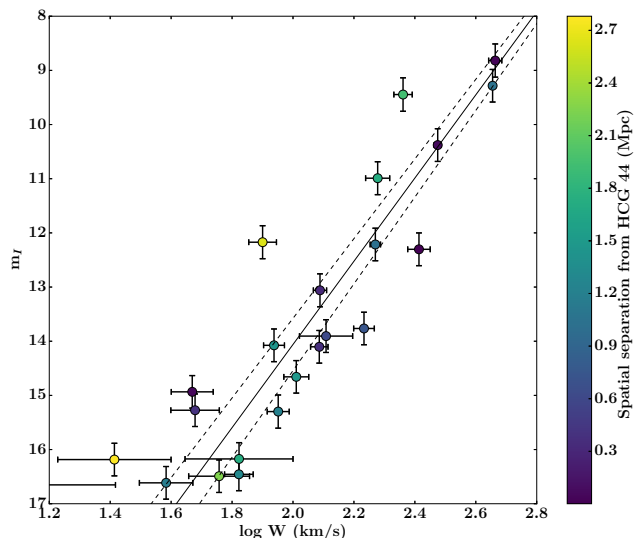


**Figure 9.** Tully Fisher relation for the galaxies within the  $2 \times 10^{13} M_{\odot}$  caustic curves within  $R=3$  Mpc of HCG 44, demonstrating the difficulty of TF methods for determining group distance. The observed sources are consistent with all being at the same distance, but due to the lack of qualifying sources with current survey data, this result is simply suggestive. Optical data were taken from the NASA-Sloan Atlas, and combined with the H I data from ALFALFA. The sample was corrected and culled following the procedure outlined in Giovanelli et al. (1997a), and discussed in section 5.3. The black line is the I-band relation from Giovanelli et al. (1997c) for a distance of 25 Mpc, with the dashed lines representing the  $1\sigma$  TF error budget discussed in Giovanelli et al. (1997b). The color axis represents the distance of the source from the center of HCG 44.

73% of the galaxies with measured redshifts in NBG 21-6), and significantly bluer than the average SDSS population. Moreover, sources within the NGC 3190 and NGC 3227 groups may be slightly more processed than the other galaxies in the region. ALFALFA detects 81% of the 43 galaxies outside the two group, compared with 63% of the 36 galaxies inside the groups, while examination of the colour distribution hints of that galaxies in the two groups appear to be somewhat redder than the other sources in the region (though this result is only marginally significant: a KS test on the two colour distributions gives  $p = 0.08$ ). The largest galaxies near the centers of the NGC 3190 and NGC 3227 groups appear to be the reddest sources in the region, and indeed, Appleton et al. (2014) discuss the importance of the green valley colour of NGC 3226, demonstrating that the colour cannot be explained by a recent resurgence of star formation, but rather must result from quenching of fairly recent star formation.

These observations together paint an observational picture that mirrors recent simulations of group and cluster formation in a hierarchical context. HCG 44, which shows the largest velocity spread in the region (NGC 3185 and NGC 3187 are separated by  $\sim 360 \text{ km s}^{-1}$ ), sits at the bottom of a larger potential well, with the other members of NGC 3190 delivering gas as they fall in. The merging pair NGC 3226/3227 rests near the bottom of a smaller potential that is falling toward the NGC 3190 well. Currently out of

equilibrium, the region will continue to group and virialize as it makes its journey toward the Virgo cluster.

The lack of primary distance information and the poorly populated nature of these groups cautions against over-interpretation of the current data, since without accurate distance measurements, the possibility remains that velocity crowding gives the appearance of connection between unrelated sources. Further, in a hierarchical model, it is possible that interactions play a significant role in increasing the velocity dispersion of the NGC 3190 and NGC 3227 groups, effecting mass estimates. However, this caution suggests important synergies between upcoming optical surveys (which can deliver more and better understood primary distance measurements), and upcoming sensitive, wide field H I surveys in understanding this fortuitously aligned group, and others like it.

## 6 CONCLUSIONS

In this paper we presented sensitive, wide-field H I imaging of the NBG 21-6 region of the Leo Cloud of galaxies, observed as part of the ALFALFA H I survey, and follow up imaging of several regions using WSRT. We detect intra-group plumes that each extend over  $\sim 2$  degrees ( $\sim 600 \text{ kpc}$ ), far beyond the primary beams of current synthesis telescopes. These features reveal interactions on larger scales than initially anticipated, providing an important tool for future modeling the recent history of these systems.

Specifically, the main conclusions of this paper are:

(i) The detection of multiple  $>300 \text{ kpc}$  H I appendages in a  $2 \times 2 \text{ Mpc}$  area of the sky mapped by ALFALFA. We find that the large gas tail to the north of HCG 44 detected in Serra et al. (2013) is likely associated with NGC 3162, as speculated by those authors, and find a tentative detection of a second, superimposed tail associated with NGC 3187 and UGC 5574. We additionally find the H I plumes in the NGC 3227 group presented in Mundell et al. (1995) extend far beyond the observed primary beam, and report the detection of a third, clumpier feature to the NE of the system, which displays a prominent kink in WSRT observations, suggestive of additional interactions.

(ii) H I features without associated stellar counterparts make up a significant component of the group gas content in the groups considered here. The intra-group gas makes up 10% of the NGC 3190 group and 40% of the NGC 3227 group.

(iii) The NGC 3190 group (containing HCG 44) and the NGC 3227 group may be part of a larger, dynamically young region experiencing active infall, and may merge in  $\sim 3\text{--}4 \text{ Gyr}$ . Examination of the broader group dynamics and optical colours suggests that its relatively local proximity and projection on the sky make the NBG 21-6 region an important laboratory for studying the role of ongoing galaxy interactions in the progression of group galaxies from the blue cloud to the red sequence.

Our observations emphasize the importance of wide-field, high sensitivity H I mapping. These massive, extended H I features were found in a region that had been extensively studied in H I; without the powerful combination of sensitivity, resolution, and field of view of ALFALFA we would

not have been able to trace galaxy interactions in these large scales. Wide field, deep mapping with next generation H I detectors like the Square Kilometer Array Pathfinders (see Giovanelli & Haynes 2016) will be necessary for a full understanding of galactic evolution in the group environment.

## ACKNOWLEDGEMENTS

The authors acknowledge the work of the entire ALFALFA collaboration in observing, flagging, and extracting sources in this field. The ALFALFA team at Cornell is supported by NSF grants AST-0607007 and AST-1107390 to RG and MPH and by grants from the Brinson Foundation. EAKA is supported by TOP1EW.14.105, which is financed by the Netherlands Organisation for Scientific Research (NWO). The authors would like to thank the referee for useful comments that helped improve the quality of the paper. LL would like to thank Michael G. Jones and Gregory Hallenbeck for several useful discussions.

This research used data from the Sloan Digital Sky Survey, funded by the Alfred P. Sloan Foundation, the participating institutions, the National Science Foundation, the U.S. Department of Energy, the National Aeronautics and Space Administration, the Japanese Monbukagakusho, the Max Planck Society, and the Higher Education Funding Council for England.

The Westerbork Synthesis Radio Telescope is operated by the ASTRON (Netherlands Institute for Radio Astronomy) with support from the Netherlands Foundation for Scientific Research (NWO).

## REFERENCES

Amanullah R., et al., 2010, *ApJ*, **716**, 712  
 Appleton P. N., et al., 2014, *ApJ*, **797**, 117  
 Bekki K., Couch W. J., 2011, *MNRAS*, **415**, 1783  
 Blakeslee J. P., Lucey J. R., Barris B. J., Hudson M. J., Tonry J. L., 2001, *MNRAS*, **327**, 1004  
 Borthakur S., Yun M. S., Verdes-Montenegro L., 2010, *ApJ*, **710**, 385  
 Borthakur S., Yun M. S., Verdes-Montenegro L., Heckman T. M., Zhu G., Braatz J. A., 2015, *ApJ*, **812**, 78  
 Bournaud F., Duc P.-A., 2006, *A&A*, **456**, 481  
 Cannon J. M., et al., 2015, *AJ*, **149**, 72  
 Garcia A. M., 1993, *A&AS*, **100**, 47  
 Geller M. J., Huchra J. P., 1983, *ApJS*, **52**, 61  
 Giovanelli R., Haynes M. P., 2016, *A&ARv*, **24**, 1  
 Giovanelli R., Haynes M. P., Herter T., Vogt N. P., Wegner G., Salzer J. J., da Costa L. N., Freudling W., 1997a, *AJ*, **113**, 22  
 Giovanelli R., Haynes M. P., Herter T., Vogt N. P., da Costa L. N., Freudling W., Salzer J. J., Wegner G., 1997b, *AJ*, **113**, 53  
 Giovanelli R., Haynes M. P., da Costa L. N., Freudling W., Salzer J. J., Wegner G., 1997c, *ApJ*, **477**, L1  
 Giovanelli R., et al., 2005, *AJ*, **130**, 2598  
 Haynes M. P., Giovanelli R., Chincarini G. L., 1984, *ARA&A*, **22**, 445  
 Haynes M. P., et al., 2011, *AJ*, **142**, 170  
 Heisler J., Tremaine S., Bahcall J. N., 1985, *ApJ*, **298**, 8  
 Hess K. M., Wilcots E. M., 2013, *AJ*, **146**, 124  
 Hibbard J. E., van der Hulst J. M., Barnes J. E., Rich R. M., 2001a, *AJ*, **122**, 2969  
 Hibbard J. E., van Gorkom J. H., Rupen M. P., Schiminovich D., 2001b, in Hibbard J. E., Rupen M., van Gorkom J. H., eds,

Astronomical Society of the Pacific Conference Series Vol. 240, Gas and Galaxy Evolution. p. 657 ([arXiv:astro-ph/0110667](#))  
 Huchra J. P., Geller M. J., 1982, *ApJ*, **257**, 423  
 Janowiecki S., et al., 2015, *ApJ*, **801**, 96  
 Jones M. G., Papastergis E., Haynes M. P., Giovanelli R., 2016, *MNRAS*,  
 Karachentsev I. D., Nasonova O. G., Karachentseva V. E., 2015a, *Astrophysical Bulletin*, **70**, 1  
 Karachentsev I. D., Tully R. B., Makarova L. N., Makarov D. I., Rizzi L., 2015b, *ApJ*, **805**, 144  
 Lee-Waddell K., Spekkens K., Haynes M. P., Stierwalt S., Changelur J., Chandra P., Giovanelli R., 2012, *MNRAS*, **427**, 2314  
 Lee-Waddell K., et al., 2014, *MNRAS*, **443**, 3601  
 Lelli F., et al., 2015, *A&A*, **584**, A113  
 Makarov D., Karachentsev I., 2011, *MNRAS*, **412**, 2498  
 Martin A. M., Giovanelli R., Haynes M. P., Saintonge A., Hoffman G. L., Kent B. R., Stierwalt S., 2009, *ApJS*, **183**, 214  
 Mould J. R., et al., 2000, *ApJ*, **529**, 786  
 Mundell C. G., Pedlar A., Axon D. J., Meaburn J., Unger S. W., 1995, *MNRAS*, **277**, 641  
 Mundell C. G., James P. A., Loiseau N., Schinnerer E., Forbes D. A., 2004, *ApJ*, **614**, 648  
 Postman M., Geller M. J., 1984, *ApJ*, **281**, 95  
 Rand R. J., 1994, *A&A*, **285**  
 Saintonge A., 2007, *AJ*, **133**, 2087  
 Sancisi R., Fraternali F., Oosterloo T., van der Hulst T., 2008, *A&ARv*, **15**, 189  
 Sault R. J., Teuben P. J., Wright M. C. H., 1995, in Shaw R. A., Payne H. E., Hayes J. J. E., eds, Astronomical Society of the Pacific Conference Series Vol. 77, Astronomical Data Analysis Software and Systems IV. p. 433 ([arXiv:astro-ph/0612759](#))  
 Serra P., et al., 2012, *MNRAS*, **422**, 1835  
 Serra P., et al., 2013, *MNRAS*, **428**, 370  
 Serra P., et al., 2015, *MNRAS*, **452**, 2680  
 Shostak G. S., Allen R. J., 1980, *A&A*, **81**, 167  
 Stierwalt S., Haynes M. P., Giovanelli R., Kent B. R., Martin A. M., Saintonge A., Karachentsev I. D., Karachentseva V. E., 2009, *AJ*, **138**, 338  
 Szabó G. M., Sárneczky K., Vinkó J., Csák B., Mészáros S., Székely P., Bebesi Z., 2003, *A&A*, **408**, 915  
 Tago E., Einasto J., Saar E., Tempel E., Einasto M., Vennik J., Müller V., 2008, *A&A*, **479**, 927  
 Tonry J. L., Dressler A., Blakeslee J. P., Ajhar E. A., Fletcher A. B., Luppino G. A., Metzger M. R., Moore C. B., 2001, *ApJ*, **546**, 681  
 Toribio M. C., Solanes J. M., Giovanelli R., Haynes M. P., Martin A. M., 2011, *ApJ*, **732**, 93  
 Tully R. B., 1987, *ApJ*, **321**, 280  
 Turner E. L., Gott III J. R., 1976, *ApJS*, **32**, 409  
 Verdes-Montenegro L., Yun M. S., Williams B. A., Huchtmeier W. K., Del Olmo A., Perea J., 2001, *A&A*, **377**, 812  
 Walker L. M., Johnson K. E., Gallagher S. C., Privon G. C., Kepley A. A., Whelan D. G., Desjardins T. D., Zabludoff A. I., 2016, *AJ*, **151**, 30  
 Wang J., et al., 2013, *MNRAS*, **433**, 270  
 Yang Y., Hammer F., Fouquet S., Flores H., Puech M., Pawlowski M. S., Kroupa P., 2014, *MNRAS*, **442**, 2419  
 Yoshii Y., Kobayashi Y., Minezaki T., Koshida S., Peterson B. A., 2014, *ApJ*, **784**, L11  
 Yun M. S., Ho P. T. P., Lo K. Y., 1994, *Nature*, **372**, 530

This paper has been typeset from a  $\text{\LaTeX}$  file prepared by the author.

<sup>1</sup> NGC 3190 is referred to as NGC 3189 in some papers. According to Serra et al. (2013), NGC3189 is the southeast component of NGC 3190.

**Table 1.** Galaxies in the NGC 3227 Group. Column 1: ID Number from the Arecibo General Catalog; column 2: alternate name; column 3: RA and Dec correspond to the optical center of each galaxy, except for H I only features, where the coordinates give the position of the peak flux; column 4: heliocentric optical recessional velocity. For all sources detected in H I, the value is from the ALFALFA catalog, else the value is from the Arecibo General Catalog; column 5: H I line width from ALFALFA, measured at the 50% flux level; note that AGC 5620 and H I<sub>North</sub> are blended, so the fluxes contain addition systematic uncertainty; column 6:  $\int SdV$  as measured in the ALFALFA data; column 7:  $\int SdV$  as measured in synthesis data, corrected for primary beam attenuation; column 8: Source of the synthesis measurement. Sources labelled L16 are from WSRT measurements presented in this paper, and those labeled M95 are VLA measurements from [Mundell et al. \(1995\)](#); column 9: H I Masses assume a distance of 25 Mpc for all sources; column 10: Fraction of group H I,  $F_{\text{H I,galaxy}}/F_{\text{H I,group}}$ , in percent. \*Classified as a member of the NGC 3190 group by [Makarov & Karachentsev \(2011\)](#) †Classified as a background source by [Makarov & Karachentsev \(2011\)](#) Note: Sources below the horizontal line are not detected at the ALFALFA sensitivity limit, which is a function of  $W_{50}$  and the rms at the position of the source (see eq. 2 in [Haynes et al. \(2011\)](#)). For a 50 km s<sup>-1</sup> wide source, the average 4 $\sigma$  ALFALFA flux upper limit is 0.3 Jy-km/s, which translates into a fractional limit of <0.6% of the total group mass for each undetected source.

| AGC                   | Name     | Coordinates<br>J2000 | cz<br>km s <sup>-1</sup> | W <sub>50</sub><br>km s <sup>-1</sup> | $F_{\text{H I,ALFA}}$<br>Jy-km s <sup>-1</sup> | $F_{\text{H I,SYN}}$<br>Jy-km s <sup>-1</sup> | Source | $\log M_{\text{H I}}$<br>$M_{\odot}$ | $f_{\text{H I}}$<br>% |
|-----------------------|----------|----------------------|--------------------------|---------------------------------------|--|---|--------|--------------------------------------|-----------------------|
| (1)                   | (2)      | (3)                  | (4)                      | (5)                                   | (6)  | (7)   | (8)    | (9)                                  | (10)                  |
| 5590*                 | NGC 3213 | 10:21:17.4+19:39:04  | 1347±1                   | 134±2                                 | 1.62±0.06                                      |   |        | 8.38                                 | 3.2                   |
| 5620                  | NGC 3227 | 10:23:30.5+19:51:53  | 1126±2                   | 412±3                                 | 17.52±0.10                                     | 14.5  | M95    | 9.41                                 | 35.0                  |
| 5629*                 |          | 10:24:12.9+21:03:01  | 1238±1                   | 113±2                                 | 3.58±0.06                                      |   |        | 8.72                                 | 7.2                   |
| 5653                  | I610     | 10:26:28.3+20:13:42  | 1168±2                   | 296±4                                 | 1.64±0.06                                      |   |        | 8.38                                 | 3.3                   |
| 5675                  | M+327047 | 10:28:30.0+19:33:46  | 1106±1                   | 83±2                                  | 4.55±0.06                                      |   |        | 8.83                                 | 9.1                   |
| 202045†               | D568-04  | 10:20:56.1+20:09:21  | 1557±2                   | 73±4                                  | 1.31±0.04                                      |   |        | 8.29                                 | 2.6                   |
| H I <sub>NE</sub>     |          | 10:25:37.4+20:20:34  | 1210±2                   | 57±4                                  | 10.18±0.21                                     | 9.61±0.39                                     | L16    | 9.18                                 | 20.3                  |
| H I <sub>North</sub>  |          | 10:23:25.7+20:00:01  | 1305±33                  | 134±16                                | 2.88±0.16                                      | 3.3   | M95    | 8.63                                 | 5.8                   |
| H I <sub>South</sub>  |          | 10:22:50.5+19:27:48  | 1292±5                   | 49±5                                  | 6.77±0.21                                      | 5.12±0.2                                      | L16    | 9.00                                 | 13.5                  |
| NGC 3227 group total: |          |                      |                          |                                       |  |   |        | 9.87                                 | 1.0                   |
| 5617                  | NGC 3226 | 10:23:27.0+19:53:54  | 1275                     | ...                                   | ...  |   |        | ...                                  | ...                   |
| 718673                |          | 10:23:15.4+20:10:40  | 1151                     | ...                                   | ...  |   |        | ...                                  | ...                   |
| 718681                |          | 10:23:21.6+20:01:38  | 1166                     | ...                                   | ...  |   |        | ...                                  | ...                   |
| 718719                |          | 10:24:34.7+20:01:57  | 1028                     | ...                                   | ...  |   |        | ...                                  | ...                   |
| 718778                |          | 10:26:31.0+20:16:60  | 1163                     | ...                                   | ...  |   |        | ...                                  | ...                   |
| 739353                |          | 10:23:22.4+19:54:51  | 1338                     | ...                                   | ...  |   |        | ...                                  | ...                   |
| 739467                |          | 10:27:37.5+20:04:43  | 1268                     | ...                                   | ...  |   |        | ...                                  | ...                   |



**Table 2.** Galaxies in the NGC 3190 Group. Column Definitions are the same as Table 1. Note that, as in Table 1, distance dependent parameters are calculated using a distance of 25 Mpc for all sources. Measurements labeled S13 are WSRT measurements from [Serra et al. \(2013\)](#). Note that AGC 5556 and 5559 are blended in the ALFALFA data. For a 50 km s<sup>-1</sup> wide source, the average 4 $\sigma$  ALFALFA flux upper limit of 0.3 Jy-km/s, translates into a fractional limit of <0.4% of the total group mass for each undetected source. \*Classified as a member of the NGC 3227 group by [Makarov & Karachentsev \(2011\)](#) †Classified as a background source by [Makarov & Karachentsev \(2011\)](#).

| AGC                   | Name                  | Coordinates<br>J2000 | cz<br>km s <sup>-1</sup> | W <sub>50</sub><br>km s <sup>-1</sup> | $F_{\text{H I,ALFA}}$<br>Jy-km s <sup>-1</sup> | $F_{\text{H I,SYN}}$<br>Jy-km s <sup>-1</sup> | Source | log $M_{\text{H I}}$<br>$M_{\odot}$ | $f_{\text{H I}}$<br>% |
|-----------------------|-----------------------|----------------------|--------------------------|---------------------------------------|--|---|--------|-------------------------------------|-----------------------|
| (1)                   | (2)                   | (3)                  | (4)                      | (5)                                   | (6)  | (7)   | (8)    | (9)                                 | (10)                  |
| 5510                  | NGC 3162              | 10:13:31.6+22:44:13  | 1302±1                   | 177±2                                 | 30.48±0.08                                     |   |        | 9.65                                | 40.0                  |
| 5524                  | 123-027               | 10:14:21.8+22:07:28  | 1636±1                   | 180±2                                 | 2.73±0.07                                      |   |        | 8.60                                | 3.6                   |
| 5544                  | NGC 3177              | 10:16:34.0+21:07:23  | 1310±2                   | 181±4                                 | 3.76±0.07                                      | 2.11  | S13    | 8.74                                | 4.9                   |
| 5554                  | NGC 3185              | 10:17:38.6+21:41:16  | 1230±1                   | 253±2                                 | 3.58±0.08                                      |   |        | 8.72                                | 4.7                   |
| 5556                  | NGC 3187              | 10:17:47.9+21:52:23  | 1586±2                   | 219±4                                 | 11.19±0.09                                     | 8.22  | S13    | 9.22                                | 14.7                  |
| 5559                  | N3189/90 <sup>†</sup> | 10:18:05.5+21:49:51  | 1310±4                   | 463±7                                 | 4.53±0.12                                      | 4.0   | S13    | 8.82                                | 5.9                   |
| 5574                  | M+425001              | 10:19:43.0+22:27:06  | 1462±5                   | 130±10                                | 2.30±0.08                                      |   |        | 8.53                                | 3.0                   |
| 5575                  |                       | 10:19:46.9+22:35:39  | 1471±3                   | 123±5                                 | 1.28±0.07                                      | 0.84  | S13    | 8.28                                | 1.7                   |
| 200162                | 123-024               | 10:12:52.5+22:43:21  | 1285±11                  | 128±23                                | 1.48±0.07                                      |   |        | 8.34                                | 1.9                   |
| 200255*               | 124-001               | 10:19:01.5+21:17:01  | 1083±3                   | 50±6                                  | 2.65±0.06                                      |   |        | 8.59                                | 3.5                   |
| 201052 <sup>†</sup>   |                       | 10:17:23.3+21:47:58  | 1943±1                   | 42±3                                  | 2.38±0.06                                      | 1.03  | S13    | 8.55                                | 3.1                   |
| 201174                | F500-4                | 10:19:19.2+22:42:05  | 1573±3                   | 51±6                                  | 0.57±0.06                                      |   |        | 7.92                                | 0.7                   |
| 201337                | 123-035               | 10:17:39.5+22:48:35  | 1178±3                   | 183±7                                 | 1.20±0.08                                      |   |        | 8.25                                | 1.6                   |
| 202134                | Wa5                   | 10:10:32.8+22:00:40  | 1280±12                  | 79±25                                 | 0.37±0.06                                      |   |        | 7.74                                | 0.5                   |
| HI <sub>Main</sub>    | T <sub>N</sub>        | 10:18:05.4+22:31:27  | 1302±5                   | 115±3                                 | 7.66±0.43                                      | 2.79  | S13    | 9.05                                | 10.1                  |
| NGC 3190 group total: |                       |                      |                          |                                       |  |   |        | 10.05                               | 1.0                   |
| 5562                  | NGC 3193              | 10:18:24.9+21:53:36  | 1378                     | ...                                   | ...  |   |        | ...                                 | ...                   |
| 208748                | 124-001b              | 10:19:00.8+21:16:55  | 1085                     | ...                                   | ...  |   |        | ...                                 | ...                   |
| 208761                |                       | 10:19:28.6+21:11:24  | 1381                     | ...                                   | ...  |   |        | ...                                 | ...                   |
| 718513                |                       | 10:17:17.6+22:09:39  | 1423                     | ...                                   | ...  |   |        | ...                                 | ...                   |
| 718530                |                       | 10:18:22.8+21:23:31  | 1408                     | ...                                   | ...  |   |        | ...                                 | ...                   |
| 718531                |                       | 10:18:40.9+21:22:49  | 1289                     | ...                                   | ...  |   |        | ...                                 | ...                   |